MICROFLUIDIC BIO-SENSOR DEVELOPMENT FOR CLINICAL APPLICATIONS: REMOVAL OF TERATOMA-FORMING CELLS FOR SAFE DERIVATION OF STEM CELL TRANSPLANTS AND EARLY DIRECT DETECTION OF LYME DISEASE

A Dissertation

Presented to the Faculty of the Graduate School

of Cornell University

in Partial Fulfillment of the Requirements for the Degree of

Doctor of Philosophy

by

Kyle Matthew Wellmerling

August 2021

© 2021 Kyle Matthew Wellmerling

ALL RIGHTS RESERVED

MICROFLUIDIC BIO-SENSOR DEVELOPMENT FOR CLINICAL APPLICATIONS: REMOVAL OF TERATOMA-FORMING CELLS FOR SAFE DERIVATION OF STEM CELL TRANSPLANTS AND EARLY DIRECT DETECTION OF LYME DISEASE

Kyle Matthew Wellmerling, Ph.D.

Cornell University 2021

Microfluidic devices have revolutionized the the field of cell biology. As microfluidic devices became affordable and mainstream, they began to serve as miniature labs for detecting and studying biological phenomenon. We develop microfluidic devices for two different biological applications in this thesis. In Chapter 2, we develop a microfluidic device for removal of rare, teratoma-forming cells from human-induced pluripotent stem cell-derived neural progenitors (hiPSC-NPCs). Though generalizable to other cell types, we begin by characterizing the differentiation process of human-induced pluripotent stem cells (hiPSCs) into neural progenitor cells (NPCs) based off residual pluripotency signature and investigate device performance by removing residual teratoma-forming cells. In Chapter 3, we develop a platform for mimicking the early stages of Lyme transmission and apply our device towards detecting *Borellia burgdorferi*, the causative agent of Lyme Disease. Early research on Lyme disease suggested a model in which the outer surface protein OspA is expressed by *Borrelia* in the tick, while outer surface protein OspC is expressed in the mammalian host. We first develop a culture system for recreating this dynamic change in surface protein expression, and then demonstrate our device is capable of capturing and detecting *Borellia burgdorferi*.

Teratoma formation remains a safety concern in therapeutic cells derived from

hiPSCs. Residual Teratoma forming cells are present in small numbers in differentiated hiPSC cultures and yet are of significant roadblock to the manufacturing and clinical translation of stem cell therapies. Rare cells are often difficult to remove with standard flow cytometry or magnetic bead sorting techniques. Here, we first characterized time-dependent expression of a teratoma marker, stage-specific embryonic antigen 5 (SSEA-5), which binds the H type-1 glycan during neural differentiation of hiPSCs. The fraction of cells SSEA-5+ remained high at 97% on day 3, dropped to 70% on day 4, 40% by day 6, and down to 1% on day 12 of differentiation, indicating successful differentiation. We engineered a microfluidic geometrically enhanced differential immunocapture (GEDI) technology to remove SSEA-5+ rare cells from hiPSC-derived neural progenitor cells (hiPSC-NPCs). The GEDI chip removed more than 95% of teratoma-forming cells and presents a facile tool to potentially functionalize with multiple antibodies and robustly enhance hiPSC-derived cell population safety prior to therapeutic transplantation. The approach is potentially amenable to generate a wide variety of high-quality therapeutic cells and can be integrated within the pipeline of cell manufacturing to improve patient safety and reduce the cost of manufacturing through early removal of undesirable cell types.

Lyme Disease is a multisystem infectious disease caused by the *Borellia burgdorferi* complex, and is a growing threat to public health. Approximately 476,000 people are infected with Lyme in the United States each year. Although Lyme is readily treated with antibiotics when detected early, early detection remains difficult. Current testing remains difficult because the standard 2-tiered ELISA assay indirectly detects Lyme via measurement of a host immune response, which suffers from an inherent time-lag in host antibody production. A direct test for Lyme Disease would overcome these inherent limitations. To this end we report

on the first microfluidic immunocapture device for Lyme Disease. We engineered a geometrically enhanced differential immunocapture (GEDI) technology to capture whole-organism *Borrelia* for direct on-chip detection. This approach is potentially amenable with other work in the field to develop direct PCR tests for Lyme Disease, as our device could serve as a platform to drastically enhance the concentration of present *Borrelia* into a small volume.

BIOGRAPHICAL SKETCH

Kyle Wellmerling grew up in the Columbus Ohio area and attended the Ohio State University, where he studied Mechanical Engineering and German. While attending Ohio State, Kyle worked several internship: one at pH Matter LLC in Columbus, and another at Ford Motor Company in Detroit Michigan. During his senior year at Ohio State Kyle performed undergraduate research in Dr. Shaurya Prakash's micro and nanofluidics lab. Guidance from his boss at pH Matter and Dr. Prakash led Kyle to pursue a doctoral degree.

Kyle joined the Micro/Nanofluidics laboratory at Cornell University led by Dr. Brian Kirby, where he became interested in developing devices for biological applications. His work has broadly focused on detecting rare cells with microfluidic immunocapture devices, and he has gained expertise in cell biology, biological assay development, and microfluidic device design and engineering.

This thesis is dedicated to my family, my friends, and all the people I met and who kept in touch along the way. Thank you to all for their contributions to my life that got me to where I am.

ACKNOWLEDGEMENTS

A doctoral student learns not where their thoughts come from, but simply learns how to take them into reality. I would like to thank my advisor, Dr. Brian Kirby, for his mentorship and persistent questioning which built me into the researcher I am today. I have appreciated his flexibility, support, and patience while pursuing my interests. I would also like to thank the other members of my thesis committee, Drs. Ben Cosgrove and Ankur Singh, for their advice and guidance. In particular, collaborations with Dr. Singh and his generous help on the teratoma project.

I would also like to thank my research colleagues, particularly Kirbylab mates that were key in providing support and consistent inquiry into my research. Thank you also to Paula Miller for her diligence and competence in keeping the Kimball laboratory running smoothly and safely. I would also like to acknowledge the excellent staff at the Imaging facility of the Biotechnology Resource Center. I would also like to thank Dr. Marcia Sawyer for her guidance through the administrative aspects of graduate school. Finally I would like to thank Dr. Tyler Kirby for his generous help in teaching me how to culture stem cells.

Many colleagues have supported or helped me in the last six years. I owe many thanks to Dr. Fredrik Thege, who guided me as I began my research in Kirbylab; Dr. Tim Lannin and Dr. Prateek Sehgal for their helpful discussions; Rachel George for her persistent optimism and energy, Mackenzie Harnett for her open questioning; Pranav Sundaram, Andrew Sanchez, Andrew Kang, Regan Stephenson, Kate Polhemus, and Anjana Jayaraman for their good fellowship and support. To the many other colleagues and friends I've made in Ithaca, thank you.

Of course, I would also like to thank my family, my good friends, and roommates. Without your support I would never have finished.

TABLE OF CONTENTS

Biographical Sketch . . . iv
Dedication . . . v
Acknowledgements . . . vi
Table of Contents . . . vii
List of Tables . . . ix
List of Figures . . . x

1 Introduction **1**

2 Microfluidic chip for label-free removal of teratoma-forming cells **5**
2.1 Abstract . . . 5
2.2 Introduction . . . 6
2.3 Methods . . . 9
2.3.1 Device fabrication and functionalization . . . 9
2.3.2 Cell Culture . . . 10
2.3.3 Flow cytometry . . . 10
2.3.4 Capture Experiments . . . 11
2.3.5 On-Chip Immunofluorescence . . . 12
2.3.6 GEDI Effluent ImmunoFluorescence . . . 12
2.3.7 Statistics . . . 14
2.4 Results and Discussion . . . 14
2.4.1 Time-dependent expression of SSEA-5 on hiPSCs and hiPSC-NPCs . . . 14
2.4.2 Microfluidic immunocapture of teratoma-forming cells . . . 16
2.4.3 Capture based on SSEA-5 expression . . . 17
2.4.4 Microfluidic Removal of SSEA-5+ Cells . . . 19
2.5 Conclusion . . . 20

3 Microfluidic Immunocapture device for direct-detection of *Borrelia* **27**
3.1 Introduction . . . 28
3.1.1 Cell Culture . . . 32
3.1.2 Capture Experiments . . . 33
3.1.3 Immunofluorescence . . . 33
3.1.4 qRT-PCR . . . 35
3.1.5 Statistics . . . 35
3.2 Results . . . 36
3.3 Discussion . . . 46
3.4 Conclusion . . . 48

4 Conclusions and future work **50**

A Supplementary Materials **52**
A.1 Supplementary materials for chapter 2 52

Bibliography **54**

LIST OF TABLES

LIST OF FIGURES

2.1 Schematic of GEDI chip and experimental procedure 23
2.2 Temporal expression of SSEA-5 on hiPSCs and hiPSC-NPCs . . . 24
2.3 GEDI-enabled capture of teratoma-forming cells from undifferentiated hiPSCs and NPCs spiked into BxPC3s. 25
2.4 GEDI-enabled capture of residual teratoma-forming cells from hiPSC-NPCs. 26

3.1 Overview of Lyme Culture system 37
3.2 Phase Contrast and external immunofluorescent images of cultured *Borrelia* 40
3.3 Phase Contrast and total immunofluorescent images of cultured *Borrelia* 41
3.4 Phase contrast and immunofluorescent images of *Borrelia*isoforms . 42
3.5 Image processing pipeline and analysis 43
3.6 *Borrelia*Immunocapture 44
3.7 On-chip immunofluorescent images of captured *Borrelia* 45

A.1 Co-expression of SSEA-3 and SSEA-5 53

CHAPTER 1

INTRODUCTION

Microfluidic devices are miniaturized fluidic systems characterized by a unique set of physics relative to conventional fluid systems. In contrast to macroscale fluid systems, microfluidic devices are almost always characterized by low Reynolds number (Re), leading to laminar and stable flow. Further, the Peclet Number (Pe), which governs the ratio of convective to diffusive transport, is often low compared to larger systems, which means the kinetics of the microfluidic system are more predictable [15]. Microfluidic device development began with the introduction of photolithography in the 1960s, with the first working inkjet printer realized in 1965. Beginning in the 1980s, the field of microfluidics truly took off as device fabrication became more mainstream. Due to the predictable dynamics of microfluidics, devices were fabricated with precise control over chemical and biological processes. This led to an explosion of devices for analyte characterization, chemical separation, rare cell capture and characterization, and eventually complex cell culture systems such as organ on a chip devices.

Kirby lab research group has developed a number of devices for rare cell capture and analysis. Of these, the geometrically enhanced differential immunocapture (GEDI) device is the most developed and widely used device. From a fluid mechanical standpoint, the device is a Hele-Shaw cell transporting high Pe number (non-diffusive) particles (individual cells). The device is designed such that cells are transported through an array of cylindrical obstacles which are functionalized with antibodies specific to the target cell population. Each obstacle in the array is offset from the previous by a defined geometry to create a staggered array, as opposed to a square array in which each obstacle is in line with the previous.

The effects of this staggered obstacle array are twofold: the staggered geometry is designed to maximize the number of collisions particles experience with the antibody-functionalized obstacles, thereby maximizing capture rate, and the obstacles increase the device surface area, meaning more antibody-functionalized surface is available for capture. In this thesis I describe two implementations of this device addressing two biological problems: 1. Removal of rare, teratoma-forming cells from hiPSC-derived neural progenitor populations, and 2. Capture of *Borellia burgdorferi* for direct detection of Lyme Disease. These two techniques bracket the spectrum of operations that can be performed with immunocapture, as negative selection is critical to eliminate teratogenic potential whereas positive selection is required for positive identification of Lyme Disease.

At present pluripotent stem cells largely remain the unrealized holy grail of regenerative medicine. Of pluripotent stem cells, hiPSCs are the most promising, as they can be patient specific, which is thought to reduce the chance for immune rejection[14, 3, 27], and does not require the sacrificing of an embryo. Although much progress has been made in the field of regenerative medicine in the last two decades, many hurdles remain before pluripotent stem cells demonstrate sufficient safety and efficacy to meet FDA requirements. Of these hurdles, tumorigenic and teratogenic potential remain a key concern[80, 4]. Tumorigenic potential here refers to the ability of stem cells to divide and self-renew indefinitely, leading to the formation of a tumor made up of a mass of cells of a similar type, while teratogenic potential refers specifically to scenario in which pluripotent stem cells spontaneously divide into a mass of cells containing cells from all three germ lines. Tumorigenic and teratogenic potential are key concerns in hiPSC therapies, because most hiPSC cell lines are derived by over-expression of known oncogenes, and hiPSCs have been shown to spontaneously de-differentiate or remain partially

differentiated following directed differentiation[80, 4].

In order to address the issue of teratogenic potential in hiPSC-derived cell populations, we engineered a GEDI immunocapture device capable of negative selection of teratoma-forming cells from hiPSC-derived NPC populations. Although a number of techniques have been attempted for the removal of teratoma-forming cells, such as sorting cells with fluorescent activated cell sorting (FACS) to filter out teratoma-forming cells or inducible suicide genes to kill transplanted cells if they begin re-expressing known oncogenes, neither have been sufficient to completely prevent teratoma formation. Further, FACS relies on pre-labeling cells with antibodies prior to sorting while suicide genes require genetic engineering; each technique requires extra safety precautions prior to FDA approval. In contrast, our method does not require pre-labeling cells with antibodies, rather cells interact with an antibody-functionalized surface for a short duration, and then are either captured out of the transplant population, or passed through the device after a short, less than 1 minute, residence time. In chapter 2 of this thesis, I describe in detail how we first validate our GEDI device for capture of hiPSCs, demonstrate the presence of cells with teratoma-forming potential in hiPSC-derived NPCs, and then show we can drastically reduce or remove the teratoma-forming potential of hiPSC-derived NPCs by filtering with our GEDI microdevice.

Whereas preventing teratoma requires negative selection of rare cells with teratogenic potential from NPC populations, identification of infection with *Borrelia* requires positive selection of rare spriochetes from typically non-bacteremic patient blood. At present, the major clinical hurdle in treating Lyme is the inability to reliably detect Lyme Disease early [53]. Current detection sensitivity during early disease stages, when Lyme is best treated, remain low, in the range of 27-90% de-

pending on the specific test and test administrator [53]. Detection remains difficult because of the nature of the detection method. The current detection method is a 2-tiered enzyme-linked immunosorbent assay (ELISA) followed by Western blot, in which a patient's overall antibody response (typically IgM and IgG antibodies) to *Borellia burgdorferi* antigens (typically whole-cell sonicate) is measured. Then, if antibody titers are above a set threshold, a second-tier immunoblot detects antibodies against a set of pre-selected *Borellia burgdorferi* protein antigens [53]. The inherent problems with this detection method are that it (1) is indirect, (2) relies on detection of patient antibodies whose production varies greatly from patient to patient, and (3) suffers from an inherent time-lag in the production of antibodies relative to infection. A method for the direct detection of *Borellia burgdorferi* would overcome these limitations and enable higher fidelity testing during early disease stages.

To address the problem of direct detection of Lyme disease we engineered the GEDI microdevice for immunocapture of *Borellia burgdorferi*. On-chip capture of *Borellia burgdorferi* can be used to directly image whole spirochetes, or as a platform to enhance cell concentration for downstream polymerase chain reaction (PCR) for detection of *Borrelia*. In order to validate our device, we first created artificial culture conditions that recreate the well-studied surface protein expression changes which occur during transmission of *Borrelia* from the tick to the mammalian host [50]. We then demonstrate that under conditions similar to early infection with Lyme we can capture and detect *Borrelia* spirochetes on-chip. I discuss this process in detail in chapter 3 of this thesis.

CHAPTER 2

MICROFLUIDIC CHIP FOR LABEL-FREE REMOVAL OF TERATOMA-FORMING CELLS

This chapter was adapted from the article:

Kyle Wellmerling and Brian Kirby. Microfluidic Chip for Label-Free Removal of Teratoma-forming Cells from Therapeutic Human Stem Cells. Journal of Immunology and Regenerative Medicine (2020) DOI: 10.1016/j.regen.2020.100030

2.1 Abstract

Teratoma formation remains a safety concern in therapeutic cells derived from human-induced pluripotent stem cells (hiPSCs). Residual Teratoma forming cells are present in small numbers in differentiated hiPSC cultures and yet are of significant roadblock to the manufacturing and clinical translation of stem cell therapies. Rare cells are often difficult to remove with standard flow cytometry or magnetic bead sorting techniques. Here, we first characterized time-dependent expression of a teratoma marker, stage-specific embryonic antigen (SSEA)-5, which binds the H type-1 glycan during neural differentiation of hiPSCs. The fraction of cells SSEA-5+ remained high at 97% on day 3, dropped to 70% on day 4, 40% by day 6, and down to 1% on day 12 of differentiation, indicating successful differentiation. We engineered a microfluidic geometrically enhanced differential immunocapture (GEDI) technology to remove SSEA-5+ rare cells from hiPSC-derived neural progenitor cells (hiPSC-NPCs). The GEDI chip removed more than 95% of teratoma-forming cells and presents a facile tool to potentially functionalize with multiple

antibodies and robustly enhance hiPSC-derived cell population safety prior to therapeutic transplantation. The approach is potentially amenable to generate a wide variety of high-quality therapeutic cells and can be integrated within the pipeline of cell manufacturing to improve patient safety and reduce the cost of manufacturing through early removal of undesirable cell types.

2.2 Introduction

Pluripotent stem cells (PSCs) represent a highly promising strategy to derive cells for therapeutic transplantation[58, 69, 76, 85, 84]. Reprogramming of somatic cells to human-induced PSCs (hiPSCs)[36] has emerged as a powerful technology for modeling diseases and as a method of generating patient-specific cells for therapeutic purposes. Differentiated cells derived from patient-specific hiPSCs are thought to be less immunogenic than tissue derived from non-allogenic human embryonic stem cells (hESCs)[14, 3, 27], circumvent the ethics of using hESCs, and self-renew indefinitely, enabling derivation of the large number of cells required for therapeutic transplantation[75].

Of tissue derived from hiPSCs, neural stem and progenitor cells are a promising therapy for treating chronic neurodegenerative diseases, for example Alzheimer's disease[61] and Parkinson's disease[40, 54]. Neural progenitor cells (NPCs) are a promising strategy to treat Alzheimer's disease and Parkinson's disease due to a widespread loss of neurons being the prevailing consequence of this diseases[87, 55, 83]. Cell transplant therapies that enhance neurogenesis or replace lost neurons may delay the progression of neurodegenerative diseases[32]. NPC grafts onto rodent models of AD demonstrate increased hippocampal synap-

tic density and increased cognitive function[7]. Additionally, cellular therapies that used fetal ventral midbrain tissue as a source of dopaminergic neurons have reported varying degrees of success[11]. However, cellular transplants utilizing fetal ventral midbrain tissue are limited due to ethical concerns of harvesting cells from donors and the inability to obtain adequate numbers of cells for transplant. hiPSC-derived NPCs (hiPSC-NPCs) are poised to overcome these obstacles and have demonstrated cell integration into host tissue[28]. In addition to chronic neurodegenerative diseases, acute neurodegeneration may result from traumatic brain injury (TBI) or spinal cord injury[39, 42, 12]. Human NPC transplantation has shown promising results to treat TBI and has demonstrated neuroprotection and improved cognitive outcomes following TBI[6]. Taken together, these results demonstrate that NPCs are a promising cellular therapy to treat acute neurodegeneration in humans. However, despite the promise of hiPSCs derived cells to treat disease, tumorigenicity of residual pluripotent-like cells in differentiated stem cells remains a concern[80, 4]. At present, numerous techniques have been applied to remove teratoma-forming potential from hiPSC-derived products, such as pretreatment with antimitotic agents and delayed transplant[49], fluorescent activated cell sorting (FACS)[86], magnetic activated cell sorting (MACS)[22], introduction of inducible suicide genes[34], and complete differentiation into mature dopaminergic neurons[19]. Unfortunately, each of these methods have limitations. Pretreatment with antimitotic agents and delayed transplant or complete differentiation into mature dopaminergic neurons increases turn-around time to derive therapeutic cells, and could make it difficult to transplant cells during the short subacute phase, during which transplantation is most efficacious[57]. Although inducible suicide genes respond in 95% of cells, they are unlikely to eliminate teratoma because as few as 2 embryonic stem cells in two million non-neoplastic cells are capable of

forming tumors in 60% of the transplants[49, 34]. Additionally, FACS and MACS have thus far proven insufficient to eliminate teratoma-forming potential and both require pre-labeling cells with antibodies, which could interfere with proliferation and differentiation[86, 22].

Microfluidic devices represent a potential avenue to remove rare, teratoma-forming cells. A wide array of microfluidic devices have been used to capture and study rare-cell populations using a variety of techniques, such as nanoparticles[**?**], open-channel micropillars[51], shallow antibody-coated microchannels[35], and magnetophoretics[64], thus poising microfluidic devices as an optimal tool for rare teratoma-forming cell capture and study. Further, our group has shown effective capture of rare circulating tumor cells (CTCs) from whole blood[41], indicating the potential of microfluidic devices to remove rare cells from a cell population. Further, microfluidic devices have demonstrated enrichment and high survivability of hiPSCs and derived neural stem cells[76]. To this end we have engineered a geometrically enhanced differential immunocapture (GEDI) chip to capture and remove rare, teratoma-forming cells from a hiPSC-NPC population by exploiting the expression of stage-specific embryonic antigen (SSEA)-5, which strongly binds the H type-1 glycan and is specifically expressed on hPSCs. To our knowledge this is the first microfluidic devices designed specifically to remove teratoma-forming cells from PSCs. The GEDI chip is designed such that cells above a set size follow a pathline through the device that maximizes the number of collisions a cell experiences with an antibody functionalized post (**Figure 1**). To remove cells from a hiPSC-NPC population, cells are first differentiated into NPCs, resuspended as single-cells, then teratoma-forming cells are captured by antibodies on the chip surface, and a purified population is obtained in the effluent (**Figure 1d**). We believe this microfluidic immunocapture represents a promising tool to address

the tumorigenic cells, potentially reduce the cell manufacturing costs by reducing post-bioprocessing of scaled-up cells and enable translation of safer stem cell therapies.

2.3 Methods

2.3.1 Device fabrication and functionalization

Devices were fabricated by A.M. Fitzgerald & Associates (Burlingame, CA) according to previously described specifications[24, 41]. The silicon device surfaces were functionalized with a previously described protocol using 3-mercaptopropyltrimethoxysilane (MPTMS) and N-gamma-maleimidobutyryloxysuccinimide ester (GMBS) NeutrAvidin-biotin chemistry (Thermo Fisher Scientific, Rockford, IL)[41, 24].The devices were functionalized with primary antibodies via a biotinylation linkage. NeutrAvidin-functionalized devices were incubated with either (1) 2 μg/mL biotinylated mouse anti-human anti-SSEA-5 antibody (Miltenyi Biotec, Bergisch Gladbach, Germany) (2) 10 μg/mL mouse anti-human anti-TRA-1-60 antibody (ThermoFisher Scientific, Waltham, MA), (3) 2 μg/mL of (1) and 10 μg/mL of (2). Control devices were functionalized with biotinylated normal (non-specific) mouse IgG antibodies ((Miltenyi Biotec, Bergisch Gladbach, Germany) at 2 μg/mL. All antibodies were prepared in 2% BSA with 1.3-1.5mM EDTA in PBS. Polydimethysiloxane (PDMS) sheets (5:1 base:curing agent), approximately 3 mm thick, were polymerized for 18 hr at 60°C and trimmed to form covers for the GEDI chip. A PDMS sheet was clamped to the top of the post arrays. Inlet and outlet holes were created with a biopsy punch, and tygon tubing was inserted

into the PDMS gasket to connect GEDI chip inlet to a syringe pump and outlet to a microcentrifuge tube for effluent collection. Devices were primed with a 50/50 Ethanol/DI water mixture, and then flushed with DI water water and PBS before experiments.

2.3.2 Cell Culture

The iPSC cell lines were provided as a kind gift by the laboratory of Jan Lammerding, and were originally generated from healthy control subjects by Elisa Di Pasquale, as described previously[17, 18]. BxPC3 cells were obtained ATCC (Manassas, VA). All cell lines were cultured in humidified incubators (37 °C and 5% CO2) using TeSR-E8 media (StemCell Technologies, Vancouver, Canada) or STEMdiff Neural Induction Medium (StemCell Technologies, Vancouver, Canada) for hiPSCs and hiPSC-NPCs respectively. hiPSC, hiPSC-NPCs, and NPCs were supplemented with 10 μM Y-27632 ROCK Inhibitor for the first day after passaging. DMEM supplemented with 10% FBS and 1% Antibiotic antimycotic for BxPC3s. hiPSCs were harvested after 3–5 days of culture at 60–80% confluency, and differentiating cells were harvested on the stated day.

2.3.3 Flow cytometry

hiPSCs or hiPSC-NPCs were trypsinized for 5–7 minutes at 37 °C and then, fixed with 4% v/v paraformaldehyde in PBS for 10-15 minutes. Cells were then permeabilized with 0.1% w/w Saponin in PBS for 5 minutes. Staining was performed with a 1:250 dilution of primary antibody and fluorescently conjugated isotype control antibody in 10% FBS in PBS blocking buffer overnight in the dark at 4°C.

Secondary fluorescent antibody was incubated for 1hr at room temperature. For data in which flow cytometry was performed directly after GEDI, cells were stained in primary antibody for 1 hour, then washed. Analysis was performed using a BD Accuri C6 flow cytometer (BD Biosciences, San Jose, CA) and Flowjo software. Cells were gated using FlowJo v10 first by identifying cells based on SSC:H vs FSC:H. Single cells were then identified by plotting FSC:A vs FSC:H and gating out cells that did not fit the main linear trend of this plot. Three biological replicates of undifferentiated hiPSCs were then fit to a normal distribution, and a cutoff threshold for counting cells as SSEA-5+ was set at just above the bottom 5% of undifferentiated hiPSCs.

2.3.4 Capture Experiments

Cells were labeled with 10μM CellTracker Dye, either Green CMFDA or Red CMPTX (Thermo Fisher Scientific, Rockford, IL) for 45 minutes, trypsinized for 5–7 minutes at 37°C and resuspended in carrier solution (2% BSA, 1.3–1.5 mM EDTA in PBS) at approximately 300 cells/mL. Precise counts for each set of experiments were obtained by counting by hand 200ul samples of each cell-suspension-running-buffer mixture. Cells were counted by hand, because more accurate counts are obtained by hand for such low cell numbers when compared with flow cytometry. In experiments in which cells were spiked into BxPC3 populations, cultures were trypsinized for 5–7 minutes at 37°C and resuspended in carrier solution at approximately 300,000 cells/mL. Functionalized silicon devices were mounted with Tygon tubing inlets and outlets in a custom PMMA holder. Cell capture was achieved by flowing 0.5 mL of cell suspension through the device at 1 mL/h followed by manual cell enumeration using fluorescence microscopy.

2.3.5 On-Chip Immunofluorescence

Cells were trypsinized for 5–7 minutes at 37°C and resuspended in carrier solution (2% BSA, 1.3–1.5 mM EDTA in PBS) at approximately 800,000-1,000,000 cells/mL. 0.5 mL of cell suspension was processed through GEDI chip functionalized with anti-SSEA-5 or normal mouse IgG (control) antibodies. Samples were fixed in 2% PFA in 50% PHEM buffer (60 mM PIPES, 25 mM HEPES, 10 mM EGTA and 2 mM MgCl2) for 15 minutes and blocked in 10% FBS in PBS for 1 hour. After staining of surface markers, the samples were permeabilized with 0.1% (w/w) Saponin. The samples were stained with, for Oct4, a primary (Abcam, ab60720,) and an AlexaFluor-488-conjugated secondary antibody (Invitrogen), for SSEA-3, a primary Rat monoclonal to SSEA-3 (Abcam, Ab16286, Lot# 1987272) and an AlexaFluor-555-conjugated secondary goat anti-rat antibody (Abcam, A21434, Lot# GR3225471-1) and, for DNA/nuclei, DAPI (Invitrogen). Samples were processed, fixed and stained within 48 h of collection.

2.3.6 GEDI Effluent ImmunoFluorescence

Three 60mm plates (Corning, CLS430166) of Day 9 hiPSC-NPCs were mixed and pumped through anti-SSEA-5 and isotype control functionalized GEDI chips at 1mL/hr for 30 minutes. The effluent of each chip (3 of each functionalization) was collected and immeditately fixed for 12 minutes in 4% w/v PFA. 70% of cells were then stained for Oct4, Nestin, and SSEA-3. 30% of cells received the corresponding secondary fluorescent antibody only. After staining, cells were pipetted and mounted onto glass coverslips coated in alginate hydrogel, to stick the fixed cells to the glass. During mounting, 2 of the secondary control slides (1 SSEA-5 and 1

isotype control) were damaged. This does not affect analysis, as secondary control cells were all lumped together for each chip functionalization condition. This is justified, because there is no reason to believe non-specific secondary antibody binding would be different between runs of different isotype control chips. Cells were then located on slides via the DAPI signal. Each slide was imaged in 3-4 locations on a Zeiss Z710 confocal microscope.

CellProfiler Image Analysis

Quantitative data was obtained by using DAPI signal to locate cells as primary objects in CellProfiler. Secondary objects were then identified using DAPI as seed locations for secondary objects. The total intensity of the secondary object (ie: Oct4 or SSEA-3 intensity) was calculated. Mean Oct4 and SSEA-3 intensity across each of the four conditions (anti-SSEA-5/positive stain, anti-SSEA-5/control stain, isotype control/positive stain, and isotype control/negative stain) for all objects was calculated, and divided by mean DAPI object area for the same condition. Secondary object size was normalized by DAPI area, due to the fact that secondary object area had high variance in the negative stain, due to poorly defined object borders (as expected). Mean secondary object positive stain fluorescence intensity normalized by mean secondary object negative stain fluorescence intensity is reported in **Figure 4**. **Figure 4** also reports the fraction of secondary objects in the positive stain that are a specified fraction brighter than the mean negative stain corresponding secondary object (ie: a threshold of 1.5 means the object is counted as positive if its integrated intensity is at least twice 1.5 times as bright as the average corresponding negative stain object.

2.3.7 Statistics

All statistical tests were performed in GraphPad 8.0. Statistical tests used are specified in figure sub-headings. Box and whiskers plots show all points, min to max, middle bar represents mean.

2.4 Results and Discussion

2.4.1 Time-dependent expression of SSEA-5 on hiPSCs and hiPSC-NPCs

To design a device that removes teratoma-forming cells from hiPSC-NPCs we first sought to characterize the differentiation dynamics of hiPSCs into NPCs. We sought to characterize how SSEA-5 expression changed during neural differentiation, as SSEA-5 was our principal marker for cells with high teratoma-forming potential[86] rather than cells solely expressing TRA-1-60. We used flow cytometry to measure single-cell SSEA-5 expression at different time points of hiPSC differentiation and measured the percent of the population SSEA-5+ at each time point of differentiation (**Figure 2a**). For each differentiation time point, we observed the fraction of cells with SSEA-5 expression above that of the bottom 5% of undifferentiated hiPSCs. We designated this fraction as SSEA-5+ (**Figure 2d**) During differentiation we noted that average SSEA-5 expression decreased dramatically throughout the 12-day differentiation period (**Figure 2b,c**). Interestingly, SSEA-5 expression dropped at discrete intervals rather than continuously during the differentiation process. SSEA-5 expression was roughly constant during the

first 3 days of neural differentiation with $97 \pm 1.9\%$ of cells remaining SSEA-5+ on day 3 (**Figure 2d**). However, by day 4 SSEA-5 expression dropped drastically such that only $69 \pm 27.8\%$ of cells were SSEA-5+. SSEA-5 expression remained relatively constant through day 6, with $40 \pm 6.03\%$ of cells SSEA-5+ on day 6. Between day 6 and day 9 however, there was a 10-fold change in the percent of cells SSEA-5+, with only $4.1 \pm 0.93\%$ of cells remaining SSEA-5+ on day 9. Between day 9 and day 12 the hiPSC-NPC population became more homogeneous, as can be seen by the narrowing of the SSEA-5 expression peak in day 12 cells compared with day 9. Further, only $1 \pm 0.06\%$ of cells remained SSEA-5+ on day 12, indicating the hiPSCs had largely completed differentiation into NPCs. We confirmed this population was not an artifact of gating or staining, as a known SSEA-5- cell population, pancreatic cancer line BxPC3, had only $0.04 \pm .03\%$ of its population SSEA-5+. Similar results were obtained with the use of a single antibody conjugated to a fluorophore to measure SSEA-5 expression (**Supplementary Figure S1a**). This indicates a small fraction of cells remain SSEA-5+ and retain teratoma-forming potential following a full time course of neural differentiation.

Next, we investigated the skew of differentiating hiPSC-NPCs populations to see if there were signs of early differentiating cells, or residual cells slow to differentiate. Interestingly, the differentiating cells were initially skewed towards low SSEA-5 expression (negative skew), indicating a few cells lose pluripotency faster than the rest of the population. Later on, however, at day 9 and day 12 (**Figure 2e**), the skew became positive (skewed towards high SSEA-5). This is in line with what would be expected for a mostly homogeneous population of differentiated cells with a few teratoma-forming cells remaining following differentiation. Finally, to corroborate flow cytometry data with immunofluorescence (IF) images (**Figure 2f**), we stained undifferentiated hiPSCs and day 9 hiPSC-NPCs with

Oct4, a master regulator of pluripotency, SSEA-5, and Nestin (a marker of neural differentiation). Strikingly, IF images corroborate flow data, clearly indicating that pockets of cells with high SSEA-5 expression remain on day 9, though with weak Oct4 expression, suggesting the cells retain partial pluripotency. Further, our results are in agreement with a study by Qiao *et al.* which found a drastic drop of pluripotency markers and increase of neural markers on day 4 of hESC neural differentiation[65]. These results may also explain the greatest variability between replicates in the day 4 group, as hiPSCs appear to undergo a drastic change between day 3 and day 4 of differentiation, which could enable greater heterogeneity between samples.

2.4.2 Microfluidic immunocapture of teratoma-forming cells

Having confirmed the presence of residual cells with expression of pluripotency markers and thus teratoma-forming potential, we sought to employ a microfluidic GEDI chip to remove the teratoma-forming cells from hiPSC-NPCs. To demonstrate SSEA-5 as a pluripotency surface marker that is capable of capturing hiPSCs on a GEDI chip, we first qualitatively compared capture on glass coverslips functionalized with anti-SSEA-5, anti-TRA-1-60, and normal mouse IgG antibodies (isotype control) (to test for steric hindrance (**Figure 3a**, as reported earlier by us[71]). We noticed similar numbers of cells on the anti-SSEA-5 and anti-TRA-1-60 coverslips compared with the isotype control functionalized cover slips. Knowing that anti-SSEA-5 and anti-TRA-1-60 coverslips can capture hiPSC, we tested functionalized GEDI chips with each of the above mentioned antibodies, either alone or in combination of anti-SSEA-5 and anti-TRA-1-60. Undifferentiated hiPSCs

were flowed through the GEDI chips using a syringe pump and at concentrations of approximately 300 cells/mL. A pass through rate was then calculated based on the number of cells counted in the effluent of each chip (ratio of number of cells in effluent to number of loaded cells). Observed pass through rates are indicated in **Figure 3b**. Whereas anti-SSEA-5 and anti-TRA-1-60 GEDI chips had similar pass through rates (4.8% and 7.2% respectively), the isotype-control GEDI chips had a much higher pass through rate (27.1%), indicating both anti-SSEA-5 and anti-TRA-1-60 GEDI chips captured hiPSCs preferentially compared with the control. Given that the anti-SSEA-5 GEDI chips had the lowest overall pass through rate, we chose to focus on this antibody for the remainder of studies in this paper.

2.4.3 Capture based on SSEA-5 expression

; After confirming SSEA-5 expression exists in differentiated hiPSC-NPCs, we sought to confirm our device's ability to remove SSEA-5+ cells from artificially mixed cell population containing SSEA-5+ and SSEA-5- cells, in a manner proportional to SSEA-5 expression level of the target population. To demonstrate this capability, we spiked hiPSC-NPCs (300 cells/mL) with a population of 300,000 BxPC3 control cells/mL. We then calculated the pass through rate for each day of differentiation (**Figure 3c**), anticipating that with differentiation the number of SSEA-5+ cells will reduce and less hiPSC-NPC will be captured on the microfluidic pillars. Indeed, we found that as the hiPSC-NPCs became further differentiated, our removal specificity reduced because there were few SSEA-5+ cells to bind to SSEA-5 antibodies on GEDI pillars (percent of spiked cells in effluent for day 9 (62.0%) and 12 (58.5%) were similar to isotype control (56.2%)). This suggested that the GEDI chip efficiently capture based on SSEA-5 expression.

To confirm the cells that were captured on the GEDI chip were pluripotent stem cells with teratoma-forming potential, we processed day 12 hiPSC-NPCs through an anti-SSEA-5 GEDI chip and also tested purified NPCs that were maintained in proliferating cultures for 2 passages (P2 NPCs). We stained cells caught on the GEDI chip for Oct4, DAPI, and SSEA-3 (a stand in for SSEA-5, due to the inability to use a secondary fluorescent antibody against SSEA-5 on chip (**supplementary figure 1b**)) (**Figure 3d**). Strikingly, nearly all of the cells, irrespective of P2-NPC or hiPSC-NPC, caught on GEDI chip co-expressed DAPI and SSEA-3. However, in the day 12 hiPSC-NPC sample, a few Oct4+ cells were captured, which were not seen in the P2 sample, indicating further differentiation in the P2 sample, as expected. In summary, these results suggest that the GEDI device captures and removes teratoma-forming cells, as cells are captured based on SSEA-5 expression, and captured cells express SSEA-3, a pluripotency marker, indicating captured cells have some pluripotency, and thus retain teratoma-forming potential. Further, when compared with other state-of-the-art methods such as inducible suicide genes, the GEDI chip removes a similar fraction of teratoma-forming cells (ie: 95% of spiked hiPSCs are removed compared with 95% success rate of suicide genes). When compared with MACS the GEDI chip outperforms MACS which only managed to remove 80% of undifferentiated hESCs[22]. Finally, although the GEDI chip performs slightly worse than a two-step MACS and cytotoxic antibody sorting method proposed by Schriebl *et al* (85-100% vs 99.1-100%)[73], the author argue direct comparison of these numbers is specious, as removing 99% of 0.1% of a cell population is more difficult than removing 99% of 5% of a cell population. In summary, this suggests the GEDI is a capable tool, able to remove teratoma-forming cells at rates similar to other methods, without requiring genetic engineering of transplant populations, or labeling transplant populations with antibodies or mag-

netic beads, which would increase the likelihood this technique actually makes it to the clinic.

2.4.4 Microfluidic Removal of SSEA-5+ Cells

Having confirmed that our device captures cells proportional to SSEA-5 expression and having confirmed the presence of rare teratoma-forming cells in differentiated populations, we quantified the effectiveness of the GEDI chip in removing teratoma- forming cells from a day 9 hiPSC-NPC population by imaging cells in the effluent of GEDI chips functionalized with anti-SSEA-5 and isotype control antibodies. The fraction of cells positive for pluripotency marker SSEA-3 was lower in the effluent obtained from anti-SSEA-5 GEDI chips than the isotype control chips for all thresholds (**Figure 4b**), indicating removal of pluripotent cells from the day 9 hiPSC-NPCs. Further, if a threshold for being SSEA-5+ is set at 50% or 100% brighter than a secondary control stain, the GEDI chip reduces the fraction of SSEA-3+ cells to 2.24% or 1.4%, respectively. This rate of pluripotency is then on par with the best reported in the literature [73]. Interestingly the fraction of OCT4+ cells was similar at low to moderate thresholds however was drastically lower for the SSEA-5 GEDI chip effluent at higher thresholds (**Figure 4c**). Further, the total fraction of Oct4+ cells was higher in day 9 hiPSC-NPCs compared with SSEA-3. A plausible explanation for the device performance is that, at low thresholds, bona fide NPCs are counted as OCT4+ cells, but at higher thresholds fewer bona fide NPCs are counted as positive, and thus residual pluripotent cells make up a larger fraction of the OCT4+ cells, of which there are more in the control GEDI chip effluent. Further, if we aggregate the average fluorescence intensity per nuclei area for the anti-SSEA-5 GEDI chips and isotype control GEDI chips

and then normalize fluorescence intensity by the respective secondary control, we find reduced pluripotency marker expression in the anti-SSEA-5 GEDI chip compared with the isotype control chip (**Figure 4a**). This indicates the anti-SSEA- 5 GEDI chips can sucessfully remove teratoma-forming cells from the day 9 hiPSC-NPC population and the effluent cells can then be potentially used for scale-up therapeutic purposes.

2.5 Conclusion

In summary, we have demonstrated that a small residual population of cells that express pluripotency markers and a specific glycan SSEA-5 exist even after prolonged periods of neural differentiation of hiPSCs. To this end, we have demonstrated a proof-of-concept study where a SSEA-5 antibody-functionalized GEDI chip can successfully reduce this teratoma-forming potential by filtering teratoma-forming cells out of the hiPSC-NPC population. We believe this work represents the first report on eliminating rare cells with teratoma-forming potential in hiPSC-derived neural stem cells with therapeutic potential. We believe that the GEDI technology is easily adaptable to other hiPSC-derived cells populations, could purify differentiated population in a label free manner, could be used to decrease turn-around time required to derive safe-therapeutic cell populations. Further we have demonstrated that hiPSCs lose SSEA-5 expression in a more punctuated or intermittent rather than continuous process, as indicated by drops in fluorescence intensity between day 3 and 6 cells and day 6 and day 9 cells. This suggests there may be optimal time-points at which to filter or sort cells prior to scale up for cell manufacturing and or therapeutic transplantation.

However, despite success in demonstrating a reduced teratoma-forming signature of cell populations filtered by our GEDI device we acknowledge the need to quantify the fraction of cells that are SSEA-5+ in the effluent of our device. We attempted to quantify the fraction of cells SSEA-5+ in day 9 hiPSC-NPCs that were filtered by an anti-SSEA-5 and isotype control GEDI chip, respectively, with flow cytometry (using a process analgous to that in **figure 2.2d**. We found on average 0.085% of the SSEA-5 chip effluent was SSEA-5+, while 0.412% of the control chip effluent was SSEA-5+. However this difference was not statistically significant (p=0.55). Future work would be to repeat more experiments of this nature and test for significance, and further to test transplanting GEDI-filtered cells into a mouse model.

Conflicts of interest

There are no conflicts to declare.

Acknowledgements

The authors would like to acknowledge funding support from the National Science Foundation award number 1511194, awarded to B.K. and A.S., and partial support from NSF CAREER award #1554275 (A.S.) The authors would like to acknowledge Tyler Kirby and Jan Lammerding for supplying the hiPSC cells and for providing training in the culture of these cells.

Author contributions statement

All experiments were performed by K.W. Pass through experiments were performed by K.W. and C.L. Data was analyzed by K.W., A.S., and B.K. Experiments were conceived by K.W., A.S., and B.K. K.W., A.S, and B.K. wrote the paper.

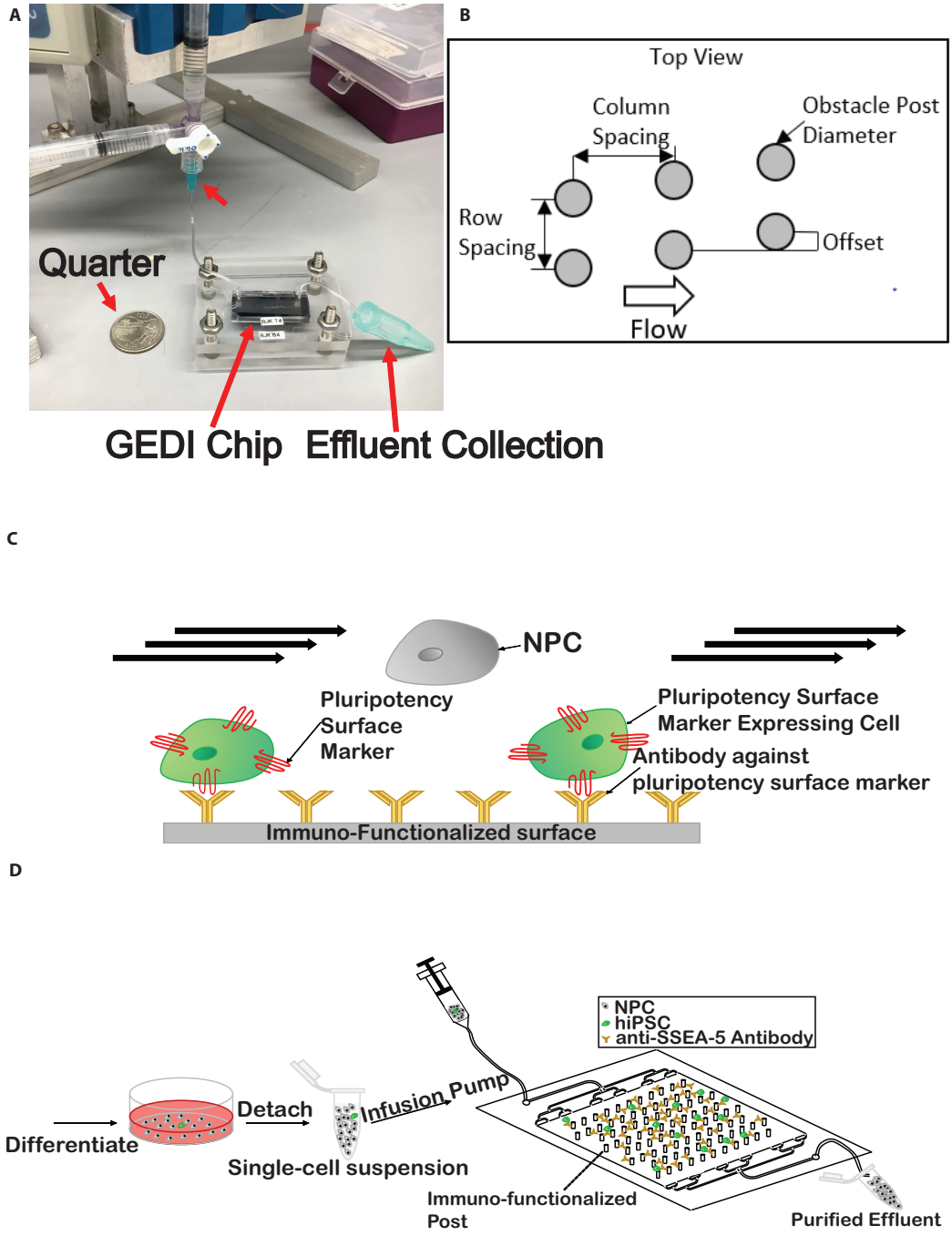

Figure 2.1: **Schematic of GEDI chip and experimental procedure**(**A**) Picture of GEDI chip setup. (**B**) GEDI chip schematic; the GEDI device consists of approximately 5000 circular posts (80µm diameter) in a 100µm deep by 8mm wide by 25mm long channel. The posts form a regular array with 100µm row spacing, and a 7µm offset[24]. (**C**) Cartoon depiction of surface functionalization. (**D**) Overview of GEDI experimental procedure.

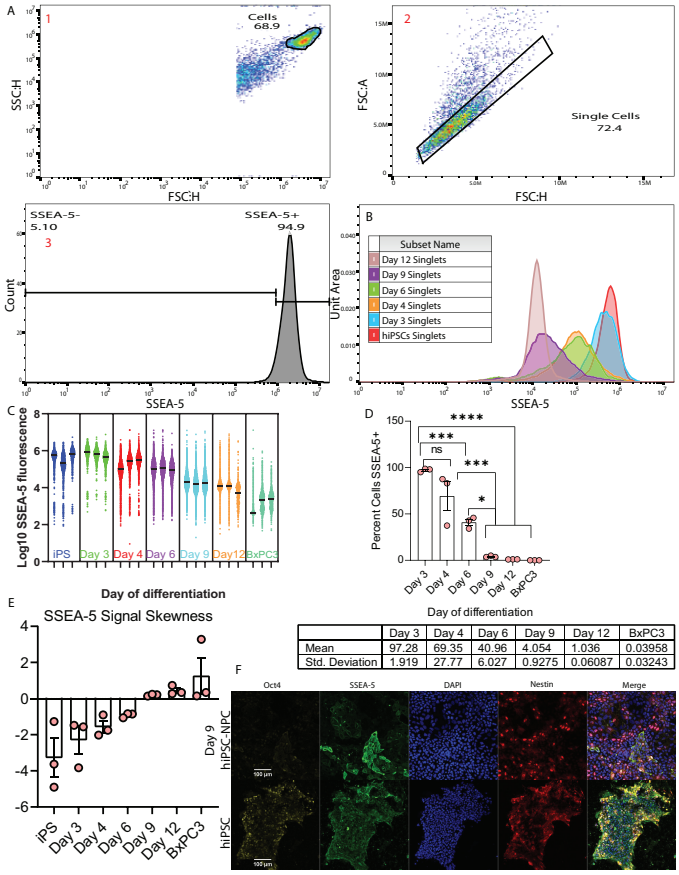

	Day 3	Day 4	Day 6	Day 9	Day 12	BxPC3
Mean	97.28	69.35	40.96	4.054	1.036	0.03958
Std. Deviation	1.919	27.77	6.027	0.9275	0.06087	0.03243

Figure 2.2: **Temporal expression of SSEA-5 on hiPSCs and hiPSC-NPCs.** (**A**) Gating of single-cells from SSC:H vs. FSC:H to identify cells, FSC:A vs FSC:H to identify single-cells, and thresholding of hiPSCs to identify SSEA-5+ cells (averaged over 3 hiPSCs populations. (**B**) SSEA-5 expression histograms for different time points of differentiation. (**C**) Log10 SSEA-5 expression for n=3 biological replicates at each time point. (**D**) Percent of cells SSEA-5$^+$ at each time point (bar represents mean), **p<.01, ***p<.001, Brown-Forsythe and Welch ANOVA tests for all tests, except Kruskal–Wallis test to compare Day 3 vs Day 9. (**E**) Skew of SSEA-5 expression at each time point (error bars represent mean with SEM). (**F**) Immunofluorescence Images of day 9 hiPSC-NPCs (top) and undifferentiated hiPSCs (bottom) (10x)(scale bar: 100μm).

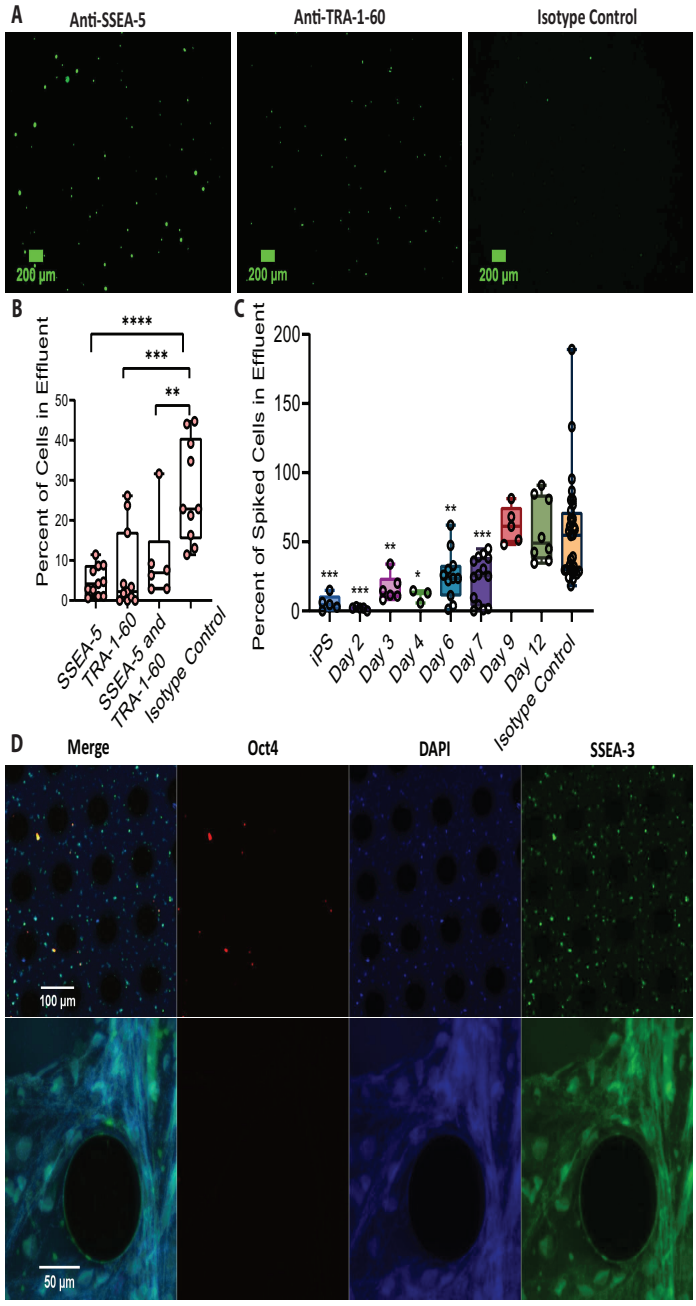

Figure 2.3: **GEDI-enabled capture of teratoma-forming cells from undifferentiated hiPSCs and NPCs spiked into BxPC3s.** (**A**) hiPSCs captured on antibody functionalized glass cover-slips. (**B**) Pass through rates for undifferentiated hiPSCs alone in suspension ****p<0.0001, ***p<0.001, **p<0.01, Tukey's multiple comparison test for all tests except SSEA-5 and TRA-1-60 compared with control, which used a Kruskal–Wallis test (n=11 for SSEA-5, TRA-1-60, n=6 SSEA-5+TRA-1-60, n=10 isotype control). (**C**) Pass through rates for hiPSC-NPCs spiked into a larger BxPC3 population at different time points of differentiaiton, Kruskal–Wallis test for all comparisons (n=5 hiPSCs, Day 2, Day 9, n=6, Day 3, n=3, Day 4, n=11, Day 6, n=14 Day 7, n=8, Day 12, n=32 Isotype Control). (**D**) Immunofluorescence images of cells captured on anti-SSEA-5 GEDI chips. Top: 10x, Day 12 NPCs; Bot: 40x, P2 NPCs (hiPSC differentiated through 2 passages as hiPSC-NPCs, then proliferated through 2 passages in a neural proliferation media.)

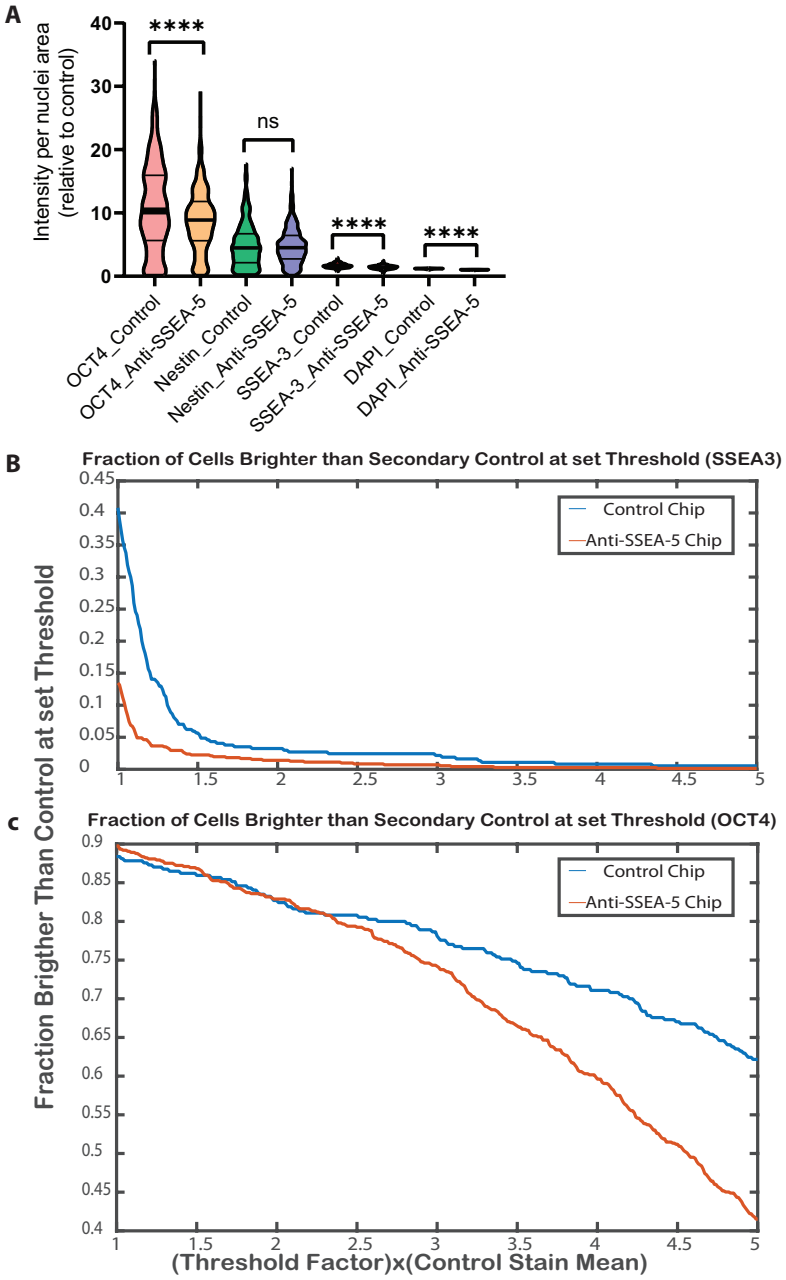

Figure 2.4: **GEDI-enabled capture of residual teratoma-forming cells from hiPSC-NPCs.** (**A**) Expression intensity per nuclei area relative to mean of secondary control for individual cells, ****p<0.0001, ns=not significant, unpaired parametric t test (n=370 cells for control, n=713 cells for anti-SSEA-5, from 3 chips of each functionalization). (**B**) Fraction of day 9 hiPSC-NPCs (a) $OCT4^+$ and (b) $SSEA\text{-}3^+$ in effluent of anti-SSEA-5 and isotype control GEDI chip at varying threshold.

CHAPTER 3

MICROFLUIDIC IMMUNOCAPTURE DEVICE FOR DIRECT-DETECTION OF *BORRELIA*

This chapter was adapted from an article submitted to scientific reports:

Kyle Wellmerling and Brian Kirby. Microfluidic Immunocapture device for direct-detection of *Borrelia*

Abstract

Lyme Disease is a multisystem infectious disease caused by the *Borellia burgdorferi* complex, and is a growing threat to public health. Approximately 476,000 people are infected with Lyme in the United States each year. Although Lyme is readily treated with antibiotics when detected early, early detection remains difficult. Current testing remains difficult because the standard 2-tiered ELISA/Western assay indirectly detects Lyme via measurement of a host immune response, which suffers from an inherent time-lag in host antibody production. A direct test for Lyme Disease would overcome these inherent limitations. To this end we report on the first microfluidic immunocapture device for Lyme Disease. We engineered a geometrically enhanced differential immunocapture (GEDI) technology to capture whole-organism *Borrelia* for direct on-chip detection. This approach is potentially amenable with other work in the field to develop direct PCR tests for Lyme Disease, as our device could serve as a platform to drastically enhance the concentration of present *Borrelia* into a small volume.

3.1 Introduction

Lyme disease is a vector-borne disease caused by the bacterial spirochete *Borellia burgdorferi*. Lyme is transmitted to humans by Ixodid ticks, primarily by the Ixodes scapularis deer tick [56]. Based on experimental studies in animals [63] and humans [21], an infected tick must feed for 48-72 hours in order to transmit *Borellia burgdorferi* to the host human. After initial infection, Lyme disease manifests in three stages: early localized, early disseminated, and late disease [56]. The early localized disease stage is characterized by the appearance of the erythema migrans rash (single or multiple) at the site of the tick bite 3 to 30 days (typically 7 to 14) after the bite. The erythema migrans (single or multiple) is found in about 90% of patients with objective evidence of infection with *Borellia burgdorferi* [56, 23, 20], and may be accompanied by systemic findings such as fever, malaise, headache, regional lymphoadenopathy, stiff neck, myalgia, and/or arthralgia. Early disseminated Lyme disease occurs after dissemination of *Borrelia* to distal sites, both through hematogenous[90] and non-hematogenous (lymphatic system or direct spread through tissue) [33] routes, and is commonly characterized by multiple erythema migrans, appearing 3-5 weeks after the tick bite and usually smaller than the primary lesion [56]. Early disseminated Lyme disease is further commonly characterized by cranial nerve palsies, facial nerve palsies, and meningitis. Other symptoms typical of early disseminated Lyme disease include: fever, myalgia, arthralgia, headache, and fatigue. Finally, late Lyme disease occurs weeks to months after initial disease transmission, and the most common manifestation is arthritis, but may also involve encephalitis, encephalopathy, and polyneuropathy. Further, people affected by late Lyme disease may develop post-treatment Lyme disease syndrome (PTLDS), also known as chronic Lyme disease.

At present approximately 30,000 cases of Lyme disease are reported to the Center for Disease Control (CDC) each year by state health departments. However, the CDC estimates that the actual number of Americans diagnosed and treated for Lyme is closer to 300,000-476,000 people per year [1]. Further, Lyme is expanding, with more regions achieving high-incidence status for Lyme Disease [43], as Lyme expands into new parts of the northern Midwest and New England regions. This spread is expected to worsen as more land is developed and chaparral is removed, and more climates become available for questing ticks owing to global climate-associated changes [81, 43].

As no currently approved human vaccine exists, early detection and treatment remain the most effective methods to manage Lyme disease. Typical treatment for Lyme in the U.S. is a 100mg dose of Doxycycline taken twice daily for two weeks [78]. Generally objective manifestations of Lyme, such as erythema migrans, meningitis, or arthritis resolve during or after completion of a course of antibiotics, but some patients report long-term (>=6 months) persistence of fatigue, musculoskeletal pain, or difficulties with concentration and memory, which are thought to be PTLDS [78]. Typically Lyme is diagnosed by the presence of erythema migrans, clinical symptoms, and patient travel or activity in Lyme-endemic areas[78, 53]. In the absence of erythema migrans, Lyme is diagnosed by a 2-tiered serologic test comprising an enzyme-linked immunoassay (ELISA) followed by a Western immunoblot. 2-tiered serologic tests, however, suffer from low sensitivity during the early disease stages, ranging anywhere from 26-89% depending on the specific test and test administrator, due largely to the time-lag in production of host antibodies [53], which typically require a couple weeks to reach detectable levels. One study reports that the standard 2-tiered serology test missed 85.7% of cases of early Lyme disease with spirochetemia [44].

Lack of a high-fidelity test for Lyme has led to misdiagnosis and heightened patient anxiety surrounding Lyme disease [56, 53]. Further, misdiagnosis leads to over prescription of antibiotics, leading to potential increases in the public health burden of Lyme. Attempts to directly detect *Borrelia* spirochetes in patients have been proposed to increase clinical Lyme testing fidelity, primarily detection via blood culture[90, 72], polymerase chain reaction (PCR) [37, 45], or a combination of the two [48, 16, 78]. However, detection by culture methods has a relatively long turnaround time to results, requiring around 7 days to achieve greater than 90% detection rate [48]. Further, culture methods would be unable to detect non-cultivable infectious spirochetes, which have been found to persist following standard antibiotic treatment [5] and make culture-based detection less efficacious.

Direct detection via immunocapture however could overcome these shortfalls, as *Borrelia* could be captured on an immunofunctionalized surface directly from a peripheral blood draw. Further, immunocapture could detect *Borrelia* regardless of whether they are replicating, so long as they express an antigen corresponding to chosen capture antibodies. Of immunocapture devices, microfluidic chips are well-poised to capture *Borrelia* directly form peripheral blood, given their long history of capturing and detecting rare cells, such as capturing circulating tumor cells from whole blood [24, 41], detecting a variety pathogens such as viruses, bacteria, fungi, or parasites [79], or rare-teratoma forming cells from differentiating stem cell populations [89].

A major defining characteristic of Lyme disease is the drastic proteome changes *Borrelia* undergoes during infection [50]. In their natural environment, *Borrelia* are transmitted from one of the four species of hard tick within the I. Ricinus complex to a mammalian host [66]. The Lyme life cycle is thought to consist

of spirochete-free tick larvae feeding on reservoir hosts: small mammals such as squirrels and mice, or birds [46, 8]. Spirochete-free larvae acquire *Borrelia* infection by feeding on reservoir hosts and then pass *Borrelia* onto new reservoir hosts during the nymphal stage or larger mammals such as deer during the adult stage [66], with humans thought to be a dead-end host. Discovery of this enzootic cycle led to a leading model in which outer surface protein A (OspA) is expressed by *Borrelia* in the tick midgut, then decreases in expression during tick bloodmeal, while another surface protein OspC increases in expression during bloodmeal, and then remains high during the early stages of host infection [74, 88, 50]]. Understanding of this cycle has been critical to preventing the spread of Lyme, as early efforts led to the development of a vaccine against OspA, which has since been pulled from the market due to a lack of efficacy [50]. Similarly, we anticipate that engineering an immune-sensor for Lyme will require validating that sensor against *Borrelia* which are representative of *Borrelia* during the early stages of mammalian infection. In this paper we first report a culture system for recreating key Osp changes associated with Lyme, then describe a microfluidic immunocapture device for the direct detection of *Borellia burgdorferi*. We report that this chip could be used for microscopic detection via a fluorescent readout, or alternatively, as a platform to enrich spirochete density for PCR detection of *Borellia burgdorferi*.

Methods

Device fabrication and functionalization

Devices were fabricated by A.M. Fitzgerald & Associates (Burlingame, CA) according to previously described specifications[24, 41]. The silicon device surfaces were functionalized with a previously described protocol using 3-mercaptopropyltrimethoxysilane (MPTMS) and N-gamma-maleimidobutyryloxysuccinimide ester (GMBS) NeutrAvidin-biotin chemistry (Thermo Fisher Scientific, Rockford, IL)[41, 24].The devices were functionalized with primary antibodies via a biotinylation linkage. NeutrAvidin-functionalized devices were incubated with 5 μg/mL biotinylated rabbit anti-*Borrelia* anti-OspC antibody (Novus Biologicals, Littleton, CO). All antibodies and chip-functionalizations were prepared in 1% BSA in PBS. Polydimethysiloxane (PDMS) sheets (5:1 base:curing agent), approximately 3 mm thick, were polymerized for 18 hr at 60°C and trimmed to form covers for the GEDI chip. A PDMS sheet was clamped to the top of the post arrays. Inlet and outlet holes were created with a biopsy punch, and tygon tubing was inserted into the PDMS gasket to connect GEDI chip inlet to a syringe pump and outlet to a microcentrifuge tube for effluent collection. Devices were primed with a 50/50 Ethanol/DI water mixture, and then flushed with DI water water and PBS before experiments.

3.1.1 Cell Culture

The B31 *Borrelia* cell lines were obtained from ATCC (Manassas VA), product number: 35210. BxPC3 cells were obtained ATCC (Manassas, VA). All cell lines

were cultured in humidified incubators (37°C and 5% CO2, pH=7.0, or 27°C, and 1% CO2, pH=8.0) using BSK-H Medium with 6% rabbit serum (Milipore Sigma, Burlington, MA). pH was adjusted by adding 6M HCL (diluted from 37% HCL (Milipore Sigma, Burlington, MA)) or Sodium hydrroxide pellets (Milipore Sigma, Burlington, MA). Media was supplemented with $100\mu g/ml$ DTT (VWR Life Sciences, Radnor, PA) and $50\mu g/ml$ Rifampicin (TCI, Montgomeryville PA). B31 were harvested after 3–7 days of culture, during the late-log to stationary growth phase.

3.1.2 Capture Experiments

Cells were centrifuged at 9800g for 10min directly from culture, and resuspended in PBS. Functionalized silicon devices were mounted with Tygon tubing inlets and outlets in a custom PMMA holder. Cell capture was achieved by flowing 0.66 mL of cell suspension through the device at 1 mL/h followed by effluent collection and a OD400 reading was obtained by distributing 200ml of either the effluent or input cell suspension into three wells of a 96-well plate, and reading optical density on a BioTek Synergy H1 plate reader.

3.1.3 Immunofluorescence

Cells were harvested from the late-log to stationary phase and centrifuged at 9,800g for 10 min in microcentrifuge tubes. All following steps were performed in micro-centrifuge tubes. Culture media was aspirated and cells were then resuspended in PBS and centrifuged through the same cycle. Cells were then resuspended in a small 200-300μL of 4% PFA in PBS and incubated for 12 min. Excess PBS (>1ml)

was used to dilute PFA solution and cells were centrifuged at 9,800g for 10min. The PFA-PBS supernatant was aspirated, and cells were resuspended in 1.5ml PBS. Cells were spun at 9,800g for 10 mins, and PBS supernatant was aspirated to remove residual 4% PFA. Cells were then either resuspended in 200-300μL 0.5% Saponin in PBS (for permeabilization stanis) or PBS, and incubated for 15mins at 37°C. Excess PBS was used to dilute permeabilization solution and cells were spun through the same cycle. A wash step with PBS followed by the same spin cycle was then performed. Cells were then blocked for 30 min at room temperature in 5% BSA in PBS. Blocking solution was removed by washing with excess PBS and spinning. Cells were then resuspended in an antibody solution containing 20μL 1% BSA in PBS, 5μL mouse anti-*Borrelia* OspA (LS Bio, Seattle, WA) (0.1mg/ml), 1μL of either rabbit anti-*Borrelia* OspC (Novus biologicals, Littleton, CO) (1mg/ml) or rabbit anti-*Borrelia* ErpN/OspE (Novus Biologicals, Littleton, CO) (1mg/ml). 2μL each of Secondary antibodies goat anti-rabbit IgG (H+L) Alexa Fluor Plus 555 (2mg/ml) and goat anti-mouse IgG (H+L) Alexa Fluor Plus 488 (2mg/ml) were added to this suspension. Antibodies were incubated overnight at 4°C for at least 18 hours. Control stains were performed similarly by replacing primary antibody volumes with a corresponding volume of 1% BSA. For experiments in which cells were stained on-chip, this antibody solution was pipeted onto dismounted GEDI chips after running, and allowed to incubate inside a humidifed chamber at 37°C for 1hr.

CellProfiler Image Analysis

Quantitative data was obtained by first flat field correcting all images in Matlab. Phase contrast images were then processed in CellProfiler to create a mask. Total intensity of OspA and OspC or OspE was then measured inside the mask and

reported as intensity per area occupied by *Borrelia*.

3.1.4 qRT-PCR

All qRT-PCR experiments were performed on a QuantStudio 3 Real-Time PCR system. A QuantiNova SYBR Green RT-PCR kit (Qiagen, Hilden Germany) was used to obtain cycle threshold (Ct) values. Samples were run in a total $20\mu L$ volume. Kit instructions form the manufacturer provided handbook were followed for all reagent volumes and cycling times, except for the denaturation, annealing and extension, and total cycles, which were 10s, 30s, and 45 cycles, respectively. Forward and reverse primers were purchased from Life Technologies Corporation (Carlsbad, CA). Forward primers for FlaB, OspA, OspC, and OspE are as follows: GATTAGCAGCGTTAATGC[62, 38], AAGTACGATCTAATTGCAACAGT[62, 38], CGGATTCTAATGCGGTTTTACTTG[33], TGATGGGCAAAGTAATG-GAGAGG [33], respectively, Citations for primers are listed after the primer. Reverse primers can be obtained by reversing the text direction.

3.1.5 Statistics

All statistical tests were performed in GraphPad 8.0. For **figure 2** statistical tests were ordinary 1-way ANOVA across all genes and days of expression. For **figure 5** a Kruskal Wallis 1-way ANOVA was used for all days in OspA external experiments, M2 in OspC external experiments, and on all days in OspE external experiments. For all other tests (ie: M4/M7 in OspC external and all total expression experiments across all days for OspA, OspC, and OspE) in **figure 5** an ordinary 1-way ANOVA was used. Asterisks are as follows: *p<.05, **p<.01, ***p<.001,

****p<.0001. All data sets were tested for normality with a D'Agostino and Pearson test when n was large enough (OspA external and total IF experiments) or a Shapiro-Wilk test when n was not large enough (all other data sets).

3.2 Results

Culture Validation

To recreate the Osp changes representative of early Lyme Disease we began by creating a culture system that mimics both tick and mammalian specific signals: temperature, pH, and atmospheric CO2 concentration (figure 1A). Previous studies have identified temperature [10, 9, 29, 59], pH of the culture medium [13], atmospheric CO2 concentration [33], or a combination of these factors [68, 67, 91] as capable of recreating many of the proteomic changes seen in host-adapted spirochetes (spirochetes cultured in dialysis membrane chambers (DMCs) inside mice or rats). For our culture system we chose a pH of 8.0, a temperature of 27°C, and an atmospheric CO2 concentration of 1% as our tick-mimicking (TM) conditions and a pH of 7.0, a temperature of 37°C, and an atmospheric CO2 concentration of 5% as our mammalian-mimicking (MM) conditions. Upon culturing *Borrelia* in the TM and MM conditions we observed several *Borrelia* isoforms, such as round bodies (RBs), blebs, and colonies (figure 1B-F). All isoforms were observed in both TM and MM conditions at all time points, suggesting the environmental factors associated with TM or MM conditions do not induce their formation. These forms have been observed by other researchers [52, 70] and are thought to play a role in stress response, antibiotic resistance, and persistence within mammalian hosts.

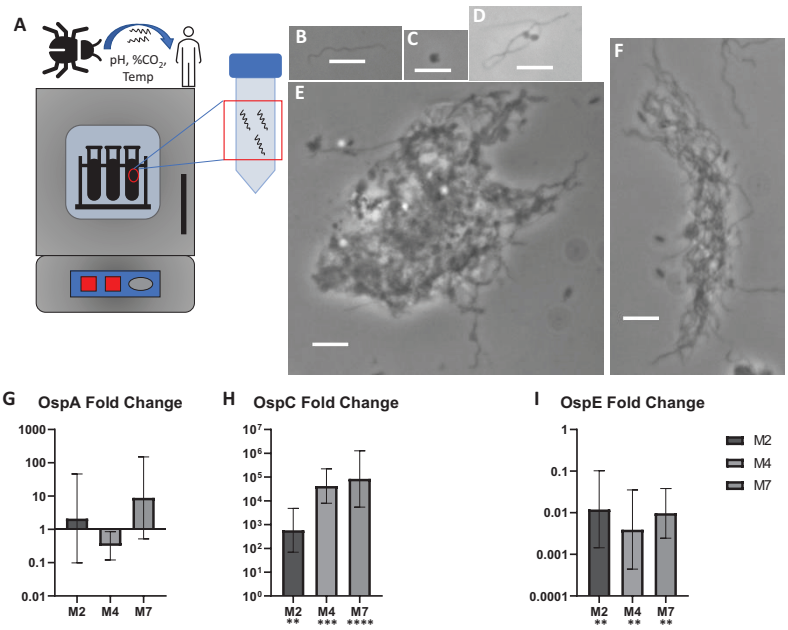

Figure 3.1: **A** Cartoon schematic depicting culture system designed to mimic environmental factors in the tick and mammalian environment. **B-F** Phase contrast images (100x) depicting *Borrelia* isoforms: spirochete (**B**), round body (**C**), bleb (**D**), and biofilm/colony (**E,F**). Scale bar is $5\mu m$. **G-I** qRT-PCR results showing fold change gene expression relative to *Borrelia* cultured in TM conditions of OspA (n=4,3,5 respectively) , OspC (n=3,3,6 respectively), and OspE (n=3, 3, 6 respectively), respectively, at 2, 4, and 7 days post transfer. (n=3 for all tick comparison data sets). Error bars show range of fold change gene expression for 1 standard deviation.

To confirm our culture system faithfully recreated Osp changes, we performed qRT-PCR experiments by culturing B31 *Borrelia* under TM conditions and then transferring *Borrelia* into MM conditions for either 2, 4, or 7 days. At the end of each time point, RNA was extracted from *Borrelia* whole-cell lysate using a Qiagen RNeasy Mini Kit and proteinase K. Quantitative reverse-transcriptase polymerase chain reaction (qRT-PCR) was then performed on extracted RNA using a QuantiNova SYBR Green RT-PCR kit on a QuantStudio 3 Real-Time PCR system. Delta delta Ct analysis [47] was then performed to determine fold-change gene expression data for OspA, OspC, and OspE at the 2, 4, and 7-day time points post transfer from the TM to MM conditions. Flagellin B (FlaB) was chosen as a control

housekeeping gene as its expression has been shown to be relatively unaffected by temperature, pH, atmospheric CO2 concentration, or cultivation inside a DMC chamber [29, 33, 67, 68, 10]. Interestingly we notice a substantial upregulation of OspC and rather sporadic changes in OspA, with no consistent trends, and a down-regulation of OspE (figure 1G-I). Although the upregulation of OspC and no substantial changes in OspA were expected, the substantial down regulation of OspE is rather surprising as it is generally understood that OspE is not expressed by *Borrelia* in the tick nor during early infection, but is upregulated during the later stages of mammalian infection [50, **?**]. However, our results suggest that our culture system does recreate the dramatic upregulation of OspC seen during early Lyme infection, and indicates that OspC is likely a good antigen choice for immunocapture, particularly given the relatively few commercially available antibodies with known target antigens.

Qualitative Immunofluorescence

Given that our qRT-PCR data indicates our culture system is recreating the population-level OspC up-regulation which occurs during early Lyme disease, we sought to further investigate the behavior of individual spirochetes with phase contrast microscopy (PCM) and immunofluorescent (IF) imaging during transmission from TM to MM conditions. Spirochete heterogeneity is known to be a substantial aspect of *Borrelia* behavior. For example, *Ohnishi et al* [60] found that *Borrelia* within unfed ticks were largely homogenous, with most producing only OspA. However, during bloodmeal many spirochetes begin producing OspC, leading to a heterogenous population with respect to OspA and OspC. Further, *Hefty et al*[30] performed a set of experiments to show that not only does *Borrelia* regulate its

surface protein expression in response environmental and host-specific factors, but also alters the cellular location of antigens during various phases of the enzootic cycle. To account for this expected heterogeneity in Osp expression we performed a set of experiments in which we stained *Borrelia* for either OspA and OspC, or OspA and OspE, then compared between samples in which *Borrelia* were surface stained (external) or permeabilized, and thus stained internally and externally (total expression). Interestingly, upon visual inspection we find *Borrelia* expressing either OspA, OspC, OspE, both OspA and OspC, both OspA and OspE, or neither (**figure 2** and **3**). We are able to find these subpopulations of *Borrelia* in either culture condition and at any time point, except MM conditions on day 7, and one group (OspA-/OspC- total stain) on day 4. Inspection of **figures 2** and **3** suggests an interesting trend: *Borrelia* become more homogenous in terms of OspA and OspC expression during later time points in mammalian conditions. Further, we note OspC expression, particularly in the externally stained samples, tends to be highly punctuated in expression. This could have implications for microfluidic device design, as the antigen-presenting surface must come into close contact with an antibody-functionalized surface.

Having investigated the heterogeneity of *Borrelia* as they transition from TM to MM conditions, we sought to investigate the heterogeneity of *Borrelia* pleomorphisms **(figure 4)**. In this investigation we sought primarily to determine which Osps were expressed externally, as only externally expressed antigens are relevant for capture. For our purposes we defined these pleomorphisms according to *Merilainen et al* [52], in which blebs consist of a spirochete with a membrane bleb, RBs consist of a lone spherical structure, and Biofilms consist of a colony mostly of spirochetes, but containing blebs and RBs. Strikingly, we observe that the Bleb and RB forms express all variations of $OspA^{+/-}/OspC^{+/-}$ and $OspA^{+/-}/OspE^{+/-}$,

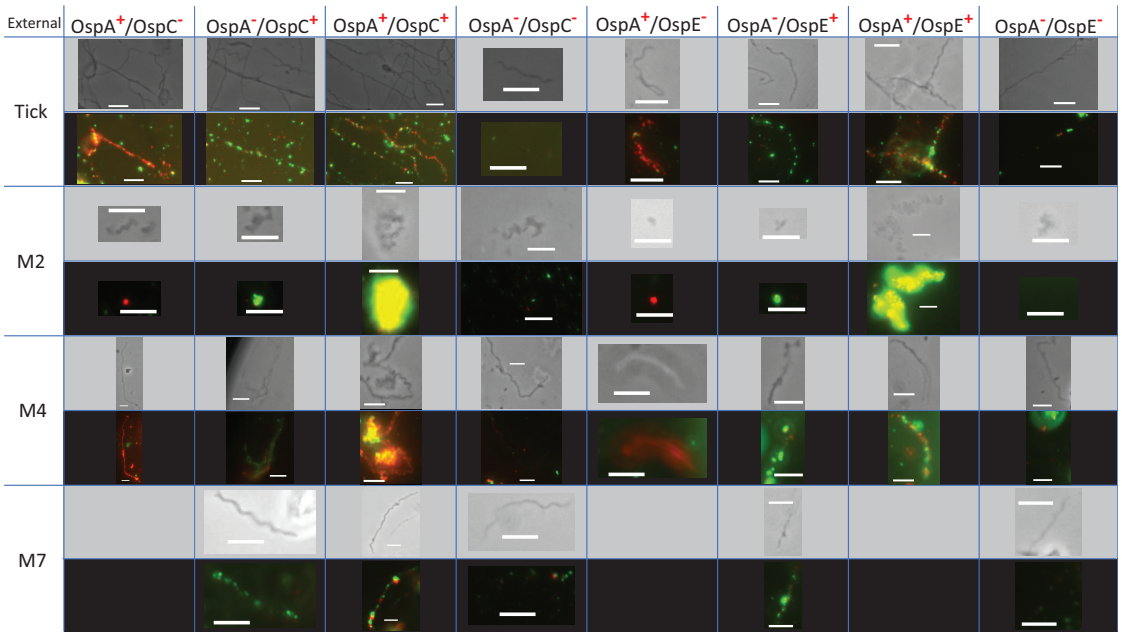

Figure 3.2: Phase contrast and corresponding immunofluorescent images (100x) showing expression of OspA and OspC, or OspA and OspE for externally stained *Borrelia*. Scale bar is $5\mu m$. Note: OspC and OspE are shown in green, OspA is shown in red.

while BioFilms/Colonies were only found to express both markers, likely due to the large number of *Borrelia* making up the colony.

Quantitative Immunofluorescence

Having qualitatively analyzed our IF images, we sought to perform a quantitative investigation of how Osp expression changes during the first week of transition from TM to MM conditions. As individual spirochetes often overlap or are entangled with several others, and given individual spirochetes are often impossible to single out within colonies, we calculated an intensity per *Borrelia* area for each image. An overview of our image processing pipeline is shown in figure 5a. In brief, it consists of taking the phase contrast (PC) image, performing a flat field correction, followed by a number of image processing algorithms which result in a mask of the PC image.

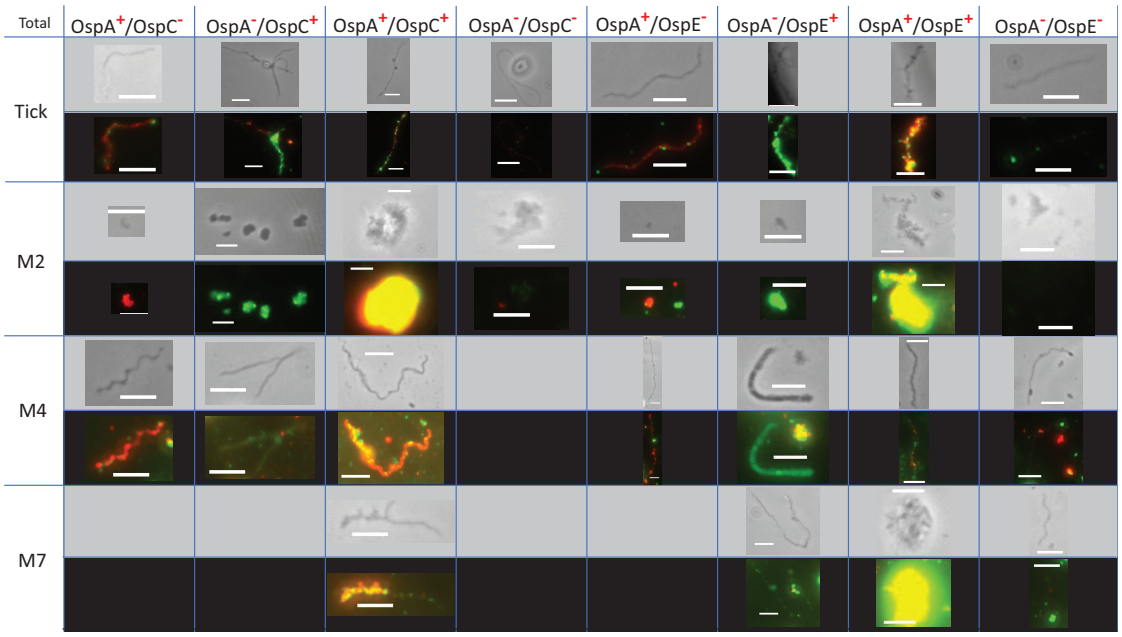

Figure 3.3: Phase contrast and corresponding immunofluorescent images (100x) showing expression of OspA and OspC, or OspA and OspE for totally stained *Borrelia*Scale bar is $5\mu m$. Note: when possible a spirochete is shown instead of an isoform. Note: OspC and OspE are shown in green, OspA is shown in red.

Each of the OspA, OspC, or OspE IF images is then multiplied by the mask so that fluorescent signal is only counted when a *Borrelia* (in any isoform) is present. Thus our image analysis shows the intensity per *Borrelia* area for each image, and does not bias against *Borrelia* with low or no expression of Osps, as masks are created from PC images. Strikingly, our results are in agreement with qRT-PCR data for OspA, as there is no consistent trend in OspA expression change during the 7 day time course. For OspE our results show little change in expression between days in MM conditions, but do not show a down-regulation relative to TM conditions. Interestingly, for OspC, we see a noticeable upregulation in OspC expression during transition from TM to MM conditions, but only for totally stained *Borrelia* and not externally stained *Borrelia* which suggests immunocapture with OspC may not necessarily be made easier by upregulation of OspC expression. However, given our qRT-PCR data suggests a strong upregulation of OspC, and OspC expression

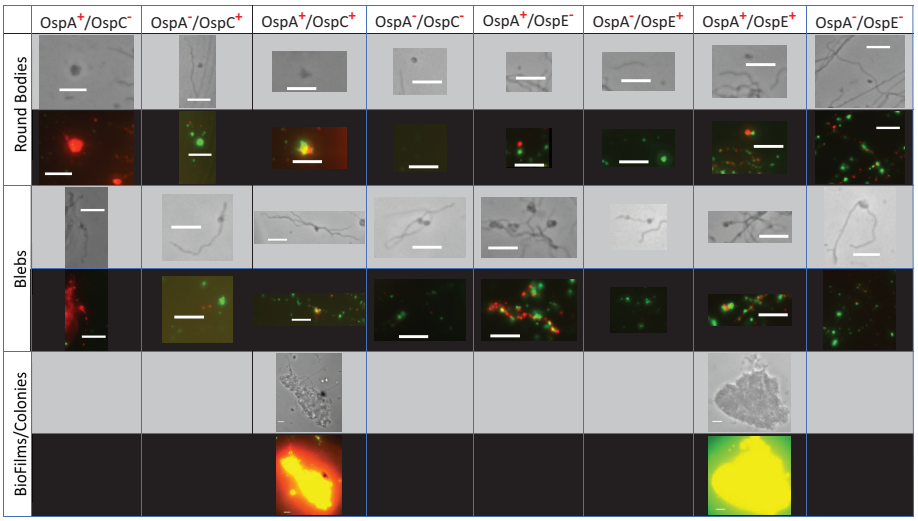

Figure 3.4: Phase contrast and corresponding immunofluorescence images (100x) showing expression of OspA and OspC, or OspA and OspE for externally stained *Borrelia* isoforms. Scale bar is 5μ m. Note: OspC and OspE are shown in green, OspA is shown in red.

is found under all conditions at all time points, and in all *Borrelia* isoforms, we chose OspC as our target capture antibody.

Immunocapture

Having decided on OspC as our target capture antibody, we first began by testing capture on a static surface in which minimal shear force is present. To perform this test *Borrelia* were seeded onto an anti-OspC functionalized glass coverslips, and allowed to bind for 5 minutes. Slides were gently washed in PBS and then imaged with PC microscopy for detection of *Borrelia*. As seen in **figure 6d** numerous *Borrelia* are found on the anti-OspC surface. Comparison to a surface functionalized with an isotype control antibody resulted in a blank coverslip (data not shown), demonstrating specificity of capture.

Having confirmed that the anti-OspC antibody is not limited by steric hin-

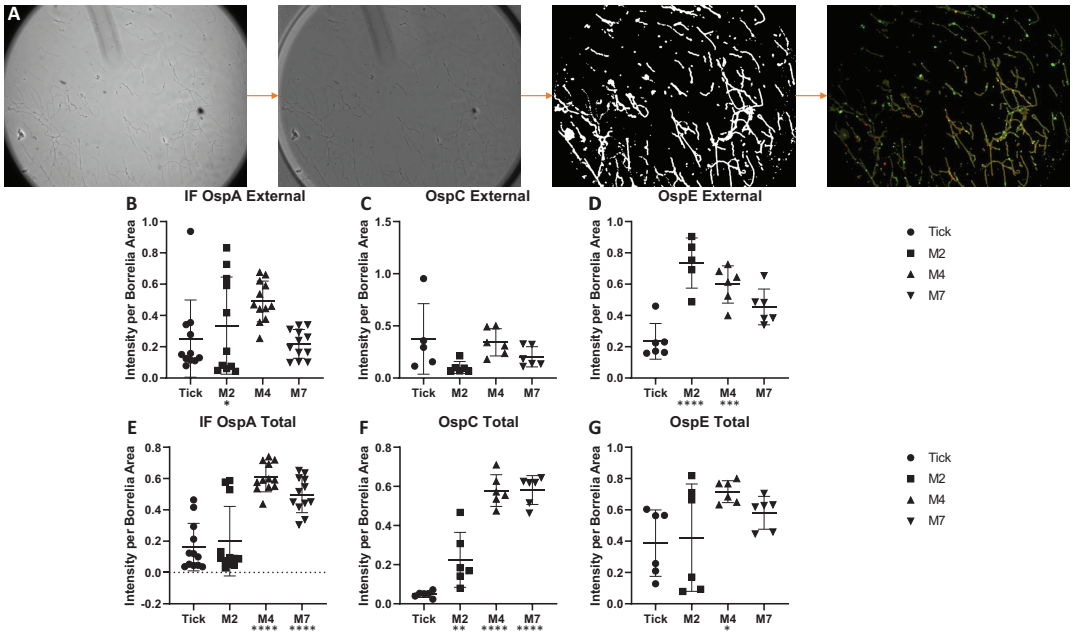

Figure 3.5: **A** Schematic depicting image analysis pipeline: raw images were flat field corrected, then masked to identify locations where *Borrelia* are present. Masked images are then multiplied by IF images so that signal is only counted in locations where *Borrelia* are present. **B-D** Graphs depicting intensity per total *Borrelia* area for OspA, OspC, and OspE. Note: each dot represents one single image (taken at 100x). Time post transfer refers to time in MM conditions after being transferred from TM conditions.

drance or lack of a readily available epitope, we began testing our microfluidic device's performance. The microfluidic immunocapture device is termed geometrically enhanced differential immunocapture (GEDI). In short, the device is a Hele-Shaw cell with a staggered obstacle array. The principle idea driving device design is that the array geometry is designed to maximize the number of collisions particles (in this case *Borrelia*) experience with an antibody-functionalized post (**figure 6b**), thus ensuring all *Borrelia* end up on a streamline which brings them in close contact with an antibody-functionalized surface. Further, the posts serve to maximize the available capture area, by drastically increasing the surface-to-volume ratio inside the microfluidic chip. For a more detailed description of device design see:[77, 25].

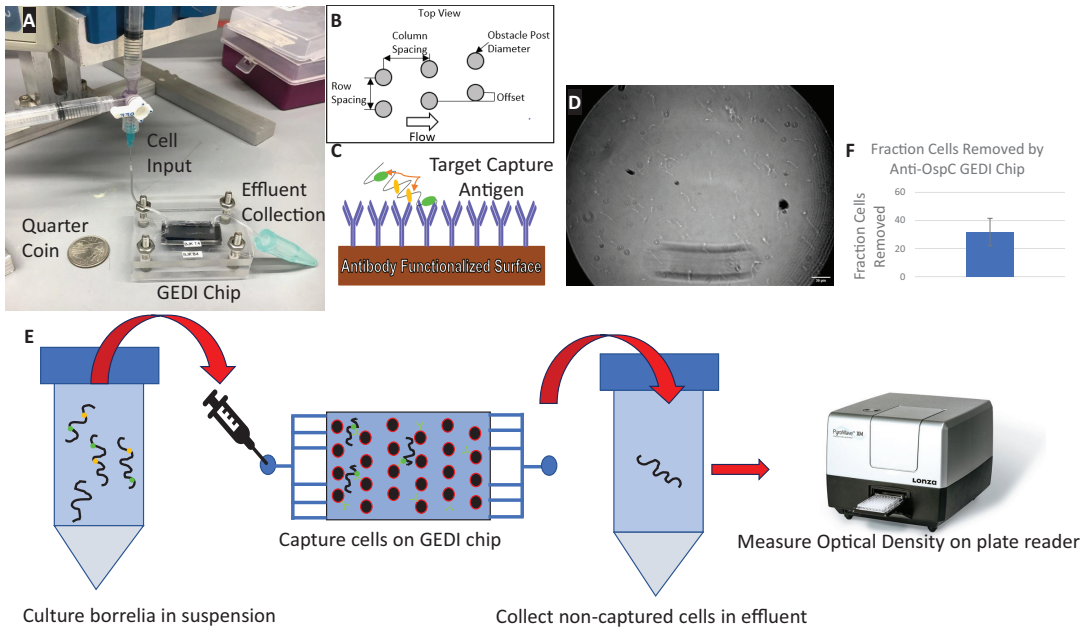

Figure 3.6: **A** Picture of GEDI chip on lab bench, note quarter for scale. **B** Schematic depicting GEDI obstacle array geometry. **C** Schematic depicting *Borrelia* capture with immuno-functionalized surface. **D** Phase contrast image of anti-OspC functionalized glass coverslip demonstrating *Borrelia* capture (40x). Scale bar is $30\mu m$. **E** Cartoon schematic depicting process for determining removal efficiency. *Borrelia* are cultured in suspension, pumped through GEDI device, effluent is collected, and OD400 is read on plate reader. **F** Graph showing fraction of cells removed by GEDI device.

To evaluate device performance, we began by taking a suspension of *Borrelia* culture and pumping that suspension through our device with an infusion pump. The effluent was then collected in a microcentrifuge tube and the optical density at 400nm (OD400) was measured on a Lonza PlateReader (**figure 6a** and **e**). By comparing the OD400 of the input cell suspension and effluent from the device, we calculated the fraction of cells removed by the GEDI chip. Our results show that on average the anti-OspC GEDI device removes 31.8% of *Borrelia* from a culture suspension grown to late-log phase under MM conditions.

After evaluating capture performance we sought to investigate Osp expression of *Borrelia* captured on chip (**figure 7b**). Interestingly we see spirochetes bound to

antibody functionalized posts (**figure 7b-c**) expressing OspC near the post, with OspA expression along the body of the spirochete (where fluid forces would pull the OspC-free spirochete body away from the post). Further, we notice our device captures a substantial number of RB *Borrelia* along the bottom surface, suggesting RBs settle to the bottom of the device due to gravitational forces, and then are captured by anti-OspC antibodies as they roll along the bottom surface (figure 7a). Further, we found our device is also capable of capturing biofilms (figure 7e) expressing a combination of OspA and OspE. We also identify both RBs and spirochetes expressing solely OspA, OspE, or both when we stained collectively for OspA and OspE. Thus on-chip imaging demonstrates our device is capable of capturing *Borrelia* isoforms expressing one of the OspA, OspC, or OspE proteins, or combination of OspA and OspC or OspA and OspE.

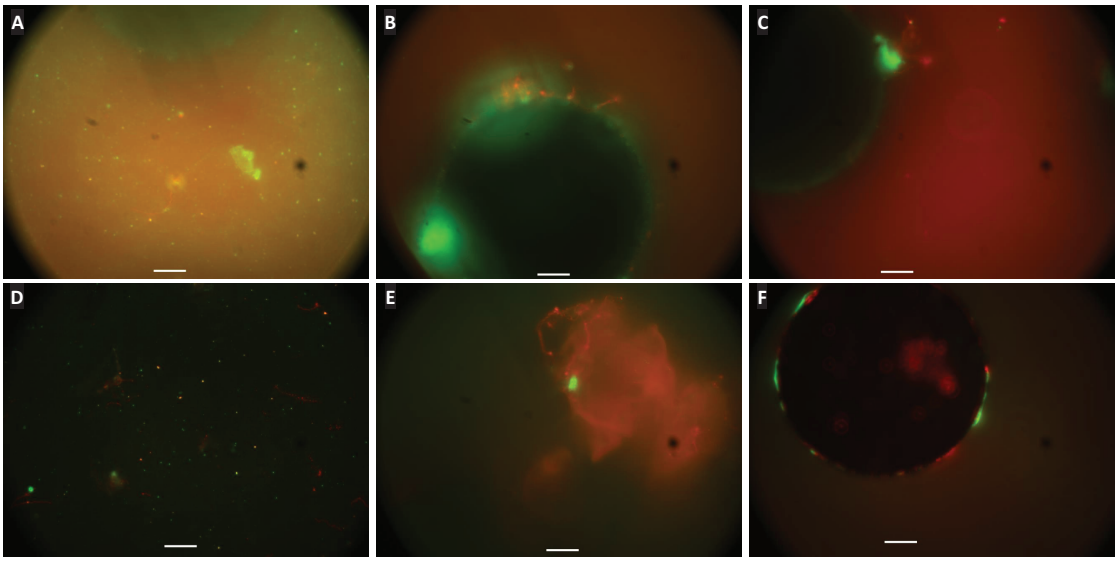

Figure 3.7: On-chip IF images showing **A** *Borrelia* RBs expressing OspC and or OspA, **B-C** Capture of OspC and OspA expressing spirochetes on obstacle post, **D** capture of *Borrelia* RBs exprssing OspE, **E** capture of *Borrelia* biofilms expressing OspA and OspE, and **F** Capture of spirochetes expressing OspA or OspE. Note: images are 100x, scale bar is $5\mu m$. Top images are OspC (green) and OspA (red), bottom images are OspE (green) and OspA (red).

3.3 Discussion

In designing a culture system that would accurately recreate Osp expression associated with the tick-to-mammalian transmission of *Borrelia* during early Lyme Disease, we chose the three environmental factors most commonly discussed in the literature which recreate the Osp changes that occur during the tick-to-mammal transition: temperature [10, 9, 29, 59], pH of culture media [13], and atmospheric CO2 concentration [33]. Although the exact literature on this topic varies with regards to exact test conditions, there is a general trend that conditions closer to those of mammalian blood (ie: 35-37C, pH =7, and 5% dissolved CO2) cause an upregulation of OspC and OspE, and either little change or down-regulation of OspA. It is interesting that our qRT-PCR results are in agreement with these trends for OspA and OspC, but are in disagreement with existing data on OspE. One possible explanation for this is that previous studies [29] have found that while a temperature shift did induce an upregulation of OspE, OspE was down-regulated in fed ticks, suggesting host-specific signals can override the positive stimulus provided by temperature [29], which could be the case for the combined effect of temperature, pH, and CO2 concentration in our culture system. In summary however, our culture system does recreate the upregulation of OspC seen from antibody response studies during early infection of canines and mice with *Borrelia* [88, 29].

Investigation of our IF images reveals substantial heterogeneity in expression of Osp proteins on individual *Borrelia*This is in line with previous studies which have found similar heterogeneity in Osp expression among *Borrelia* whether they are cultured in vitro, in DMCs, or collected from ticks [30, 60]. It is interesting to note previous studies have found the same beaded expression of OspE [**?**] as

we did but did not find the same beaded expression we observed for OspC. The cause of this heterogeneity *in vivo* is thought to arise from the role these proteins play in movement of *Borrelia* from the unfed tick midgut to the tick salivary glands during feeding. *Ohnishi et al*[60] propose a model in which non-infectious *Borrelia* expressing neither OspA or OspC, or solely OspA infect the host dermis early on during tick feeding, with *Borrelia* expressing neither OspA or OspC, or a subgroup expressing only OspC establishing stable infection in the host dermis later on. However, *Grimm et al*[26] performed a series of studies with a mutant *Borrelia* strain lacking OspC and showed OspC was required for stable infection of mice, regardless of infection route (needle or tick). A possible explanation for this discrepancy is that *Ohnishi et al*[60] investigated the mouse dermis attached to the tick hypostome rather than attempting to retrieve infectious *Borrelia* from the mouse through feeding ticks. The OspA and OspC double negative *Borrelia* detected in mouse dermis could then represent a non-infectious population of spirochetes, which would be in line with the presence of these double negative spirochetes in mice that were not stably infected [60].

These findings have a substantial impact on the design of immunocapture devices as we chose OspC as our primary capture antigen due to available data demonstrating OspC sero-reactivity across multiple mammalian species [88, 60], and although there is sero-reactivity in humans to OspC [2] behavior of *Borrelia* in humans often differs from model organisms such as mice, due to humans not being part of the natural enzootic cycle of *Borrelia*However, if future studies demonstrate a substantial fraction of infectious *Borrelia* expressing Osps other than OspC during early infection, our device performance could be enhanced by functionalizing the device with a combination of multiple *Borrelia*-specific antibodies. Further, the beaded expression pattern we observed for OspC has implications for chip design,

as it suggests that not only do *Borrelia* need to be brought in close contact with an antibody-functionalized surface, but that device performance might be enhanced by mixing of the cell suspension, so that the chance the OspC expressing surface of the *Borrelia* is brought into contact with the antibody-functionalized surface is maximized. One method of achieving this may be through incorporating the staggered herringbone mixer design developed by *Stroock et al*[82] in our GEDI device.

Of further interest is our results showing expression of OspA, OspC, and OspE among some RBs and blebs, as well as biofilms. Although we are unaware of any literature on the expression of these Osp proteins by *Borrelia* isoforms, our data is encouraging from an immunocapture perspective as on-chip imaging demonstrates that our device captures *Borrelia* in any isoform. These isoforms are thought to largely arise from a *Borrelia* stress response, particularly due to antibiotics[52, 70]. Our ability to capture these isoforms is promising as it is plausible *Borrelia* exist in one or multiple of these forms during infection in humans as they are entering into a stressful foreign environment, and would be exposed to antibiotics if the patient is actively being treated for Lyme [70].

3.4 Conclusion

In summary, our device is the first reported immunocapture device for the detection of whole-organism *Borrelia*. Although our *Borrelia* removal rate was only 31.8%, this removal rate is expected to be sufficient for positive identification of *Borrelia*. Previous studies have shown that only 78% [29] of *Borrelia* spirochetes cultured under similar conditions express OspC in vitro. Further, unbeknownst

to us at the time of experimentation, OspC expression has been shown to decrease upon repeated passage of *Borrelia* at 37°C [74]. As our capture experiments were performed on *Borrelia* passaged through MM conditions for 2-4 passages, we deem our experiments an appropriate challenge to the system's ability to capture *Borrelia* under a variety of expression conditions.

Further, although this work's results focused on IF assays to detect *Borrelia* captured on chip, our device could serve as a platform to enhance the concentration of *Borrelia* present in patient blood into a small volume, which could be combined with work by other researchers to detect *Borrelia* with PCR [45]. This approach to Lyme detection would be particularly useful given the presence of non-cultivable spriochetes in antibiotic treated mice [31, 5]. While our work lays the ground work for microfluidic immunocapture and detection of Lyme, future work should focus on three things: a multi-antibody functionalization scheme to address the heterogeneity during Lyme infection, microfluidic mixing to ensure non-uniformly expressed antigens come into contact with antibody-functionalized surfaces, and development of an on-chip PCR assay to detect captured *Borrelia*.

Author contributions statement

All experiments were performed by K.W. Writing was done by K.W. and B.K.

CHAPTER 4

CONCLUSIONS AND FUTURE WORK

In this dissertation, I have developed the GEDI microfluidic device for the removal of teratoma-forming cells from hiPSC-derived NPCs (Chapter 2), and for the direct detection of *Borellia burgdorferi* (Chapters 3). In general, both applications involved developing assays for investigating the biological behavior of cell populations, as well as creating quantitative tools for interpreting raw data.

In the first aim of this dissertation, I used flow cytometry to investigate the dynamics of hiPSCs as they differentiated into NPCs. I showed that on a whole the population loses expression of pluripotency/teratoma-forming markers, but that a small but significant fraction of the differentiated population retains expression of teratoma-forming markers. I then used confocal immunofluorescent imaging to demonstrate the presence of pockets of cells containing high expression of teratoma-forming markers within the differentiated population. I then demonstrated that the GEDI device is capable of selectively capturing and removing cells with high expression of the SSEA-5 teratoma-forming marker. Finally, I showed that the GEDI device is capable of significantly reducing the expression of teratoma-forming markers when a differentiated population of hiPSC-derived NPCs is sent through the device. Although I demonstrated the efficacy of this device for hiPSC-derived NPCs, the GEDI device and the quantitative tools I created to evaluate its performance are generalizable to any hiPSC-derived cell line, as it relies on the behavior of the hiPSC population rather than the differentiated population. Future work on this project should involve testing GEDI-sorted transplants on a mouse model for teratoma formation, and integrating our device with other stem-cell-transplant derivation methods, as our device could serve as a

filter to remove teratoma-forming cells at any stage of cell derivation, due to its label-free nature.

In the second aim of this dissertation, I developed a culture system to create outer surface protein changes representative of early infection of mammals with Lyme Disease. This culture system is critical to validating our device in a clinically-relevant setting. Further, I developed assays for the investigation and quantification of Osp expression as the *Borrelia* transition from the tick-mimicking environment to the mammalian-mimicking environment. Finally I showed that the GEDI device is capable of capturing *Borrelia* and can serve as a platform for direct detection of Lyme Disease. Further I showed our device captures *Borrelia* in any isoform, which is relevant to clinical detection as these isoforms may be present in infected humans [70]. This work is impactful because it is the first reported immunocapture device for Lyme Disease. Further, our device is readily integrable with other direct detection methods such as PCR, as our device could serve as a platform to drastically enhance the concentration of present *Borrelia* into a substantially smaller volume. Future work should involve testing our device on the blood of Lyme-positive mouse and human patients, developing a multi-antibody panel to address the heterogeneity in infectious *Borrelia* populations, and collaborating with researchers developing PCR tests for Lyme Disease.

APPENDIX A

SUPPLEMENTARY MATERIALS

A.1 Supplementary materials for chapter 2

Confirmation of SSEA-5 positivity by single-antibody stain

When quantifying the fraction of cells SSEA-5+ in the differentiating hiPSC-NPCs, we sought to confirm that our signal was not an artifact of a strong secondary fluorescent antibody. We performed a similar set of experiments with a primary-conjugated antibody to confirm that the residual teratoma-forming population is real (see figure A1).

SSEA-3 and SSEA-5 co-expression

When performing immunofluorescent stains of hiPSCs-NPCs sent through a GEDI device, we used SSEA-3 as a stand-in for SSEA-5 expression, as our chip was functionalized with SSEA-5, and we were concerned about possible secondary binding to the chip surface, or antibody de-lamination from the chip surface causing aberrant signal in the effluent. For this reason we stained cells on-chip and in the effluent with SSEA-3. Flow cytometry plots showing the co-expression of SSEA-3 and SSEA-5 by hiPSCs are presented below (figure A2).

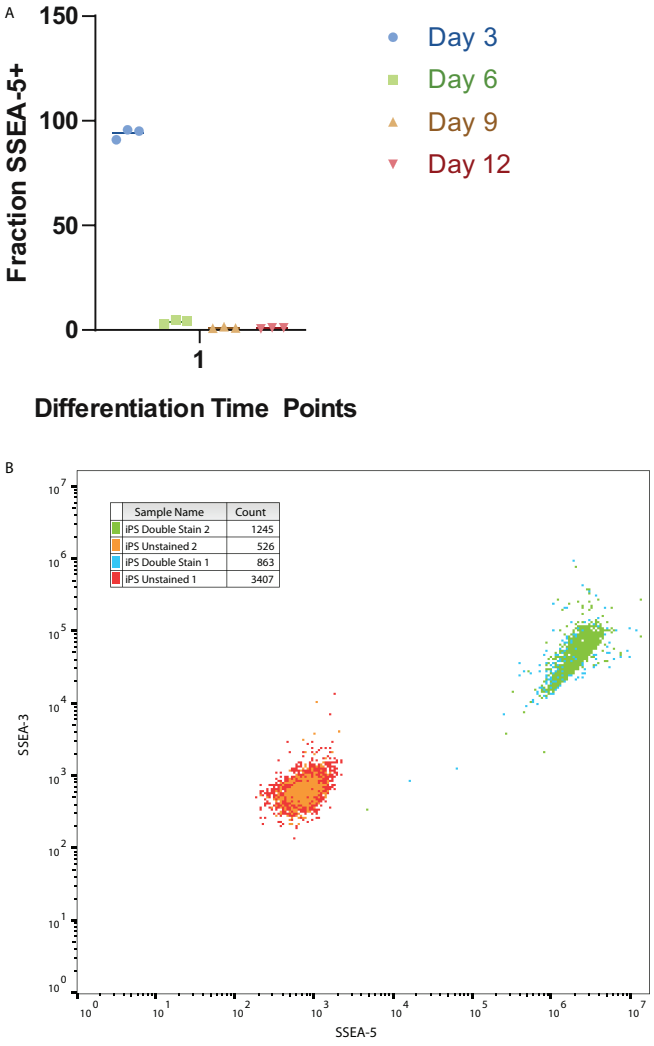

Figure A.1: **Co-expression of SSEA-3 and SSEA-5**. (a) Fraction of cells SSEA-5+ as determined by single-antibody stain. (b) A scatter plot of flow cytometry data showing co-expression of SSEA-3 and SSEA-5 by undifferentiated hiPSCs.

BIBLIOGRAPHY

[1] CDC Lyme Data and Surveillance kernel description. https://www.cdc.gov/lyme/datasurveillance/index.html. Accessed: 2021-07-16.

[2] Juan Anguita, Michael N. Hedrick, and Erol Fikrig. Adaptation of Borrelia burgdorferi in the tick and the mammalian host. *FEMS Microbiology Reviews*, 27(4):493–504, 2003.

[3] Ryoko Araki, Masahiro Uda, Yuko Hoki, Misato Sunayama, Miki Nakamura, Shunsuke Ando, Mayumi Sugiura, Hisashi Ideno, Akemi Shimada, Akira Nifuji, and Masumi Abe. Negligible immunogenicity of terminally differentiated cells derived from induced pluripotent or embryonic stem cells. *Nature*, 494(7435):100–104, 2013.

[4] Roger A. Barker, Malin Parmar, Lorenz Studer, and Jun Takahashi. Human Trials of Stem Cell-Derived Dopamine Neurons for Parkinson's Disease: Dawn of a New Era. *Cell Stem Cell*, 21(5):569–573, 2017.

[5] Stephen W. Barthold, Emir Hodzic, Denise M. Imai, Sunlian Feng, Xiaohua Yang, and Benjamin J. Luft. Ineffectiveness of tigecycline against persistent Borrelia burgdorferi. *Antimicrobial Agents and Chemotherapy*, 54(2):643–651, 2010.

[6] M.O. Blaya, P. Tsoulfas, H.M. Bramlett, and W.D. Dietrich. Neural progenitor cell transplantation promotes neuroprotection, enhances hippocampal neurogenesis, and improves cognitive outcomes after traumatic brain injury. *Experimental Neurology*, 264:67–81, 2015.

[7] Mathew Blurton-Jones, Masashi Kitazawa, Hilda Martinez-Coria, Nicholas A. Castello, Franz Josef Müller, Jeanne F. Loring, Tritia R. Yamasaki, Wayne W. Poon, Kim N. Green, and Frank M. LaFerla. Neural stem cells improve cognition via BDNF in a transgenic model of Alzheimer disease. *Proceedings of the National Academy of Sciences of the United States of America*, 106(32):13594–13599, 2009.

[8] E. M. Bosler, B. G. Ormiston, J. L. Coleman, J. P. Hanrahan, and J. L. Benach. Prevalence of the Lyme disease spirochete in populations of white-tailed deer and white-footed mice. *Yale Journal of Biology and Medicine*, 57(4):651–659, 1984.

[9] Chad S. Brooks, P. Scott Hefty, Sarah E. Jolliff, and Darrin R. Akins. Global analysis of Borrelia burgdorferi genes regulated by mammalian host-specific signals. *Infection and Immunity*, 71(6):3371–3383, 2003.

[10] Chad S. Brooks, Santosh R. Vuppala, Amy M. Jett, and Darrin R. Akins. Identification of Borrelia burgdorferi outer surface proteins. *Infection and Immunity*, 74(1):296–304, 2006.

[11] Patrik Brundin, Roger A. Barker, and Malin Parmar. Neural grafting in Parkinson's disease. Problems and possibilities. *Progress in Brain Research*, 184(C):265–294, 2010.

[12] Jessica C. Butts, Dylan A. McCreedy, Jorge Alexis Martinez-Vargas, Frederico N. Mendoza-Camacho, Tracy A. Hookway, Casey A. Gifford, Praveen Taneja, Linda Noble-Haeusslein, and Todd C. McDevitt. Differentiation of V2a interneurons from human pluripotent stem cells. *Proceedings of the National Academy of Sciences of the United States of America*, 114(19):4969–4974, 2017.

[13] James A. Carroll, Claude F. Garon, and Tom G. Schwan. Effects of environmental pH on membrane proteins in Borrelia burgdorferi. *Infection and Immunity*, 67(7):3181–3187, 1999.

[14] Arvind Chhabra. Inherent immunogenicity or lack thereof of pluripotent stem cells: implications for cell replacement therapy. *Frontiers in Immunology*, 8(AUG):1–11, 2017.

[15] Neil Convery and Nikolaj Gadegaard. 30 Years of Microfluidics. *Micro and Nano Engineering*, 2(May 2018):76–91, 2019.

[16] Peggy Coulter, Clara Lema, Diane Flayhart, Amy S. Linhardt, John N. Aucott, Paul G. Auwaerter, and J. Stephen Dumler. Two-year evaluation of Borrelia burgdorferi culture and supplemental tests for definitive diagnosis of lyme disease. *Journal of Clinical Microbiology*, 43(10):5080–5084, 2005.

[17] E. Di Pasquale, F. Lodola, M. Miragoli, M. Denegri, J. E. Avelino-Cruz, M. Buonocore, H. Nakahama, P. Portararo, R. Bloise, C. Napolitano, G. Condorelli, and S. G. Priori. CaMKII inhibition rectifies arrhythmic phenotype in a patient-specific model of catecholaminergic polymorphic ventricular tachycardia. *Cell Death and Disease*, 4(10):e843–11, 2013.

[18] Elisa Di Pasquale, Belle Song, and Gianluigi Condorelli. Generation of Human

Cardiomyocytes: A Differentiation Protocol from Feeder-free Human Induced Pluripotent Stem Cells. *Journal of Visualized Experiments*, (76):1–6, 2013.

[19] Daisuke Doi, Asuka Morizane, Tetsuhiro Kikuchi, Hirotaka Onoe, Takuya Hayashi, Toshiyuki Kawasaki, Makoto Motono, Yoshiki Sasai, Hidemoto Saiki, Masanori Gomi, Tatsuya Yoshikawa, Hideki Hayashi, Mizuya Shinoyama, Mohamed M. Refaat, Hirofumi Suemori, Susumu Miyamoto, and Jun Takahashi. Prolonged maturation culture favors a reduction in the tumorigenicity and the dopaminergic function of human ESC-derived neural cells in a primate model of Parkinson's disease. *Stem Cells*, 30(5):935–945, 2012.

[20] The New England. Journal Medicine ©. pages 209–215, 1998.

[21] The New England. of Lyme Disease After an Ixodes Scapularis Tick Bite. *English Journal*, 345(2):79–84, 2001.

[22] Chui Yee Fong, Gary S.L. Peh, Kalamegam Gauthaman, and Ariff Bongso. Separation of SSEA-4 and TRA-1-60 labelled undifferentiated human embryonic stem cells from a heterogeneous cell population using magnetic-activated cell sorting (MACS) and fluorescence-activated cell sorting (FACS). *Stem Cell Reviews and Reports*, 5(1):72–80, 2009.

[23] M Gerber, E Shapiro, G Burke, V Parcells, and G Bell. The New England Journal of Medicine LYME DISEASE IN CHILDREN IN SOUTHEASTERN CONNECTICUT. 1996.

[24] Jason P. Gleghorn, Erica D. Pratt, Denise Denning, He Liu, Neil H. Bander, Scott T. Tagawa, David M. Nanus, Paraskevi A. Giannakakou, and Brian J. Kirby. Capture of circulating tumor cells from whole blood of prostate cancer patients using geometrically enhanced differential immunocapture (GEDI) and a prostate-specific antibody. *Lab on a Chip*, 10(1):27–29, 2010.

[25] Jason P. Gleghorn, James P. Smith, and Brian J. Kirby. Transport and collision dynamics in periodic asymmetric obstacle arrays: Rational design of microfluidic rare-cell immunocapture devices. *Physical Review E - Statistical, Nonlinear, and Soft Matter Physics*, 88(3):1–9, 2013.

[26] Dorothee Grimm, Kit Tilly, Rebecca Byram, Philip E. Stewart, Jonathan G. Krum, Dawn M. Bueschel, Tom G. Schwan, Paul F. Policastro, Abdallah F. Elias, and Patricia A. Rosa. Outer-surface protein C of the Lyme disease spirochete: A protein induced in ticks for infection of mammals. *Proceedings of the National Academy of Sciences of the United States of America*, 101(9):3142–3147, 2004.

[27] Prajna Guha, John W. Morgan, Gustavo Mostoslavsky, Neil P. Rodrigues, and Ashleigh S. Boyd. Lack of immune response to differentiated cells derived from syngeneic induced pluripotent stem cells. *Cell Stem Cell*, 12(4):407–412, 2013.

[28] G. Hargus, O. Cooper, M. Deleidi, A. Levy, K. Lee, E. Marlow, A. Yow, F. Soldner, D. Hockemeyer, P. J. Hallett, T. Osborn, R. Jaenisch, and O. Isacson. Differentiated Parkinson patient-derived induced pluripotent stem cells grow in the adult rodent brain and reduce motor asymmetry in Parkinsonian rats. *Proceedings of the National Academy of Sciences*, 107(36):15921–15926, 2010.

[29] P. S. Hefty, S. E. Jolliff, M. J. Caimano, S. K. Wikel, J. D. Radolf, and D. R. Akins. Regulation of OspE-related, OspF-related, and Elp lipoproteins of Borrelia burgdorferi strain 297 by mammalian host-specific signals. *Infection and Immunity*, 69(6):3618–3627, 2001.

[30] P. Scott Hefty, Sarah E. Jolliff, Melissa J. Caimano, Stephen K. Wikel, and Darrin R. Akins. Changes in temporal and spatial patterns of outer surface lipoprotein expression generate population heterogeneity and antigenic diversity in the lyme disease spirochete, Borrelia burgdorferi. *Infection and Immunity*, 70(7):3468–3478, 2002.

[31] Emir Hodzic, Denise Imai, Sunlian Feng, and Stephen W. Barthold. Resurgence of persisting non-cultivable Borrelia burgdorferi following antibiotic treatment in mice. *PLoS ONE*, 9(1), 2014.

[32] D. H. Hwang, H. J. Lee, I. H. Park, J. I. Seok, B. G. Kim, I. S. Joo, and S. U. Kim. Intrathecal transplantation of human neural stem cells overexpressing VEGF provide behavioral improvement, disease onset delay and survival extension in transgenic ALS mice. *Gene Therapy*, 16(10):1234–1244, 2009.

[33] Jenny A. Hyde, Jerome P. Trzeciakowski, and Jonathan T. Skare. Borrelia burgdorferi alters its gene expression and antigenic profile in response to CO2 levels. *Journal of Bacteriology*, 189(2):437–445, 2007.

[34] Go Itakura, Soya Kawabata, Miki Ando, Yuichiro Nishiyama, Keiko Sugai, Masahiro Ozaki, Tsuyoshi Iida, Toshiki Ookubo, Kota Kojima, Rei Kashiwagi, Kaori Yasutake, Hiromitsu Nakauchi, Hiroyuki Miyoshi, Narihito Nagoshi, Jun Kohyama, Akio Iwanami, Morio Matsumoto, Masaya Nakamura, and Hideyuki Okano. Fail-Safe System against Potential Tumorigenicity after Transplantation of iPSC Derivatives. *Stem Cell Reports*, 8(3):673–684, 2017.

[35] Kihoon Jang, Yo Tanaka, Jun Wakabayashi, Reina Ishii, Kae Sato, Kazuma Mawatari, Mats Nilsson, and Takehiko Kitamori. Selective cell capture and analysis using shallow antibody-coated microchannels. *Biomicrofluidics*, 6(4):1–11, 2012.

[36] Corrected June and S E E Last Page. Corrected 5 june 2009; see last page. *Science*, 324(June):797–802, 2009.

[37] Lyudmila Karan, Marat Makenov, Nadezhda Kolyasnikova, Olga Stukolova, Marina Toporkova, and Olga Olenkova. Dynamics of spirochetemia and early PCR detection of Borrelia miyamotoi. *Emerging Infectious Diseases*, 24(5):860–867, 2018.

[38] Hiroki Kawabata, Hiroyuki Tashibu, Kazuto Yamada, Toshiyuki Masuzawa, and Yasutake Yanagihara. Polymerase Chain Reaction Analysis of Borrelia Species Isolated in Japan. *Microbiology and Immunology*, 38(8):591–598, 1994.

[39] Mohamad Khazaei, Christopher S. Ahuja, and Michael G. Fehlings. Induced pluripotent stem cells for traumatic spinal cord injury. *Frontiers in Cell and Developmental Biology*, 4(JAN):1–9, 2017.

[40] Tetsuhiro Kikuchi, Asuka Morizane, Daisuke Doi, Hiroaki Magotani, Hirotaka Onoe, Takuya Hayashi, Hiroshi Mizuma, Sayuki Takara, Ryosuke Takahashi, Haruhisa Inoue, Satoshi Morita, Michio Yamamoto, Keisuke Okita, Masato Nakagawa, Malin Parmar, and Jun Takahashi. Human iPS cell-derived dopaminergic neurons function in a primate Parkinson's disease model. *Nature*, 548(7669):592–596, 2017.

[41] Brian J. Kirby, Mona Jodari, Matthew S. Loftus, Gunjan Gakhar, Erica D. Pratt, Chantal Chanel-Vos, Jason P. Gleghorn, Steven M. Santana, He Liu, James P. Smith, Vicente N. Navarro, Scott T. Tagawa, Neil H. Bander, David M. Nanus, and Paraskevi Giannakakou. Functional characterization of circulating tumor cells with a prostate-cancer-specific microfluidic device. *PLoS ONE*, 7(4):1–10, 2012.

[42] Yoshiomi Kobayashi, Yohei Okada, Go Itakura, Hiroki Iwai, Soraya Nishimura, Akimasa Yasuda, Satoshi Nori, Keigo Hikishima, Tsunehiko Konomi, Kanehiro Fujiyoshi, Osahiko Tsuji, Yoshiaki Toyama, Shinya Yamanaka, Masaya Nakamura, and Hideyuki Okano. Pre-Evaluated Safe Human iPSC-Derived Neural Stem Cells Promote Functional Recovery after Spinal Cord Injury in Common Marmoset without Tumorigenicity. *PLoS ONE*, 7(12):1–13, 2012.

[43] Kiersten J. Kugeler, Grace M. Farley, Joseph D. Forrester, and Paul S. Mead. Geographic distribution and expansion of human lyme disease, United States. *Emerging Infectious Diseases*, 21(8):1455–1457, 2015.

[44] Shih Han Lee, Jennie N. Jeyapalan, Vanessa Appleby, Dzul Azri Mohamed Noor, Virginie Sottile, and Paul J. Scotting. Dynamic methylation and expression of Oct4 in early neural stem cells. *Journal of Anatomy*, 217(3):203–213, 2010.

[45] Sin Hang Lee, Veronica S. Vigliotti, Jessica S. Vigliotti, William Jones, and Suri Pappu. Increased sensitivity and specificity of Borrelia burgdorferi 16S ribosomal DNA detection. *American Journal of Clinical Pathology*, 133(4):569–576, 2010.

[46] J. F. Levine, M. L. Wilson, and A. Spielman. Mice as reservoirs of the Lyme disease spirochete. *American Journal of Tropical Medicine and Hygiene*, 34(2):355–360, 1985.

[47] Kenneth J. Livak and Thomas D. Schmittgen. Analysis of relative gene expression data using real-time quantitative PCR and the 2-$\Delta\Delta$CT method. *Methods*, 25(4):402–408, 2001.

[48] Dionysios Liveris, Ira Schwartz, Susan Bittker, Denise Cooper, Radha Iyer, Mary E. Cox, and Gary P. Wormser. Improving the yield of blood cultures from patients with early lyme disease. *Journal of Clinical Microbiology*, 49(6):2166–2168, 2011.

[49] Philippe Magown, Robert M. Brownstone, and Victor F. Rafuse. Tumor prevention facilitates delayed transplant of stem cell-derived motoneurons. *Annals of Clinical and Translational Neurology*, 3(8):637–649, 2016.

[50] Author Manuscript and Outer Surface Proteins. P . O Box 1842 Bushbuckridge 27 March 2018 APPLICATION FOR INTERN – ENVIRONMENT AND CLIMATE CHANGE PROGRAMME :. (March):2018, 2018.

[51] Taisuke Masuda, Woneui Song, Hayao Nakanishi, Wu Lei, Anas Mohd Noor, and Fumihito Arai. Rare cell isolation and recovery on open-channel microfluidic chip. *PLoS ONE*, 12(4):1–14, 2017.

[52] Leena Meriläinen, Anni Herranen, Armin Schwarzbach, and Leona Gilbert. Morphological and biochemical features of Borrelia burgdorferi pleomorphic forms. *Microbiology (United Kingdom)*, 161(3):516–527, 2015.

[53] Andrew Moore, Christina Nelson, Claudia Molins, Paul Mead, and Martin Schriefer. Current guidelines, common clinical pitfalls, and future directions for laboratory diagnosis of lyme disease, United States. *Emerging Infectious Diseases*, 22(7):1169–1177, 2016.

[54] Asuka Morizane, Tetsuhiro Kikuchi, Takuya Hayashi, Hiroshi Mizuma, Sayuki Takara, Hisashi Doi, Aya Mawatari, Matthew F. Glasser, Takashi Shiina, Hirohito Ishigaki, Yasushi Itoh, Keisuke Okita, Emi Yamasaki, Daisuke Doi, Hirotaka Onoe, Kazumasa Ogasawara, Shinya Yamanaka, and Jun Takahashi. MHC matching improves engraftment of iPSC-derived neurons in non-human primates. *Nature Communications*, 8(1):1–12, 2017.

[55] Mattson MP. Pathways towards and away from Alzheimer's disease. *Nature*, 430(7000):631–9, 2004.

[56] Thomas S. Murray and Eugene D. Shapiro. Lyme disease. *Clinics in Laboratory Medicine*, 30(1):311–328, 2010.

[57] Narihito Nagoshi and Hideyuki Okano. Applications of induced pluripotent stem cell technologies in spinal cord injury. *Journal of Neurochemistry*, 141(6):848–860, 2017.

[58] Shin-ichi Nishikawa, Robert A Goldstein, and Concepcion R Nierras. and therapy. 9(September):725–729, 2008.

[59] Marygorret Obonyo, Ulrike G. Munderloh, Volker Fingerle, Bettina Wilske, and Timothy J. Kurtti. Borrelia burgdorferi in tick cell culture modulates expression of outer surface proteins A and C in response to temperature. *Journal of Clinical Microbiology*, 37(7):2137–2141, 1999.

[60] Jun Ohnishi, Joseph Piesman, and Aravinda M. De Silva. Antigenic and genetic heterogeneity of Borrelia burgdorferi populations transmitted by ticks. *Proceedings of the National Academy of Sciences of the United States of America*, 98(2):670–675, 2001.

[61] Jay Penney, William T. Ralvenius, and Li-Huei Tsai. Modeling Alzheimer's disease with iPSC-derived brain cells. *Molecular Psychiatry*, 2019.

[62] D. H. Persing, S. R. Telford, A. Spielman, and S. W. Barthold. Detection of Borrelia burgdorferi infection in Ixodes dammini ticks with the polymerase chain reaction. *Journal of Clinical Microbiology*, 28(3):566–572, 1990.

[63] J. Piesman, T. N. Mather, R. J. Sinsky, and A. Spielman. Duration of tick attachment and Borrelia burgdorferi transmission. *Journal of Clinical Microbiology*, 25(3):557–558, 1987.

[64] Brian D. Plouffe, Madhumita Mahalanabis, Laura H. Lewis, Catherine M. Klapperich, and Shashi K. Murthy. Clinically relevant microfluidic magnetophoretic isolation of rare-cell populations for diagnostic and therapeutic monitoring applications. *Analytical Chemistry*, 84(3):1336–1344, 2012.

[65] Yunbo Qiao, Ran Wang, Xianfa Yang, Ke Tang, and Naihe Jing. Dual roles of histone H3 lysine 9 acetylation in human embryonic stem cell pluripotency and neural differentiation. *Journal of Biological Chemistry*, 290(4):2508–2520, 2015.

[66] Justin D. Radolf, Melissa J. Caimano, Brian Stevenson, and Linden T. Hu. Of ticks, mice and men: Understanding the dual-host lifestyle of Lyme disease spirochaetes. *Nature Reviews Microbiology*, 10(2):87–99, 2012.

[67] R. Ramamoorthy and D. Scholl-Meeker. Borrelia burgdorferi proteins whose expression is similarly affected by culture temperature and pH. *Infection and Immunity*, 69(4):2739–2742, 2001.

[68] Andrew T. Revel, Adel M. Talaat, and Michael V. Norgard. DNA microarray analysis of differential gene expression in Borrelia burgdorferi, the Lyme disease spirochete. *Proceedings of the National Academy of Sciences of the United States of America*, 99(3):1562–1567, 2002.

[69] Daisy A. Robinton and George Q. Daley. The promise of induced pluripotent stem cells in research and therapy. *Nature*, 481(7381):295–305, 2012.

[70] Natalie Rudenko, Maryna Golovchenko, Katerina Kybicova, and Marie Vancova. Metamorphoses of Lyme disease spirochetes: Phenomenon of Borrelia persisters. *Parasites and Vectors*, 12(1):1–10, 2019.

[71] Steven M. Santana, He Liu, Neil H. Bander, Jason P. Gleghorn, and Brian J. Kirby. Immunocapture of prostate cancer cells by use of anti-PSMA antibodies in microdevices. *Biomedical Microdevices*, 14(2):401–407, 2012.

[72] Eva Sapi, Namrata Pabbati, Akshita Datar, Ellen M. Davies, Amy Rattelle, and Bruce A. Kuo. Improved culture conditions for the growth and detection of Borrelia from human serum. *International Journal of Medical Sciences*, 10(4):362–376, feb 2013.

[73] Kornelia Schriebl, Gernalia Satianegara, Austin Hwang, Heng Liang Tan, Wey Jia Fong, Henry He Yang, Alois Jungbauer, and Andre Choo. Selective removal of undifferentiated human embryonic stem cells using magnetic activated cell sorting followed by a cytotoxic antibody. *Tissue Engineering - Part A*, 18(9-10):899–909, 2012.

[74] Tom G. Schwan and Joseph Piesman. Temporal changes in outer surface proteins A and C of the lyme disease- associated spirochete, Borrelia burgdorferi, during the chain of infection in ticks and mice. *Journal of Clinical Microbiology*, 38(1):382–388, 2000.

[75] Margarida Serra, Catarina Brito, Cláudia Correia, and Paula M. Alves. Process engineering of human pluripotent stem cells for clinical application. *Trends in Biotechnology*, 30(6):350–359, 2012.

[76] A Singh, S Suri, T Lee, J M Chilton, M T Cooke, W Chen, J Fu, S L Stice, H Lu, T C McDevitt, and A J Garcia. Adhesion strength-based, label-free isolation of human pluripotent stem cells. *Nature Methods*, 10(5):438–444, 2013.

[77] James P. Smith, Timothy B. Lannin, Yusef A. Syed, Steven M. Santana, and Brian J. Kirby. Parametric control of collision rates and capture rates in geometrically enhanced differential immunocapture (GEDI) microfluidic devices for rare cell capture. *Biomedical Microdevices*, 16(1):143–151, 2014.

[78] Gerold Stanek, Gary P. Wormser, Jeremy Gray, and Franc Strle. Lyme borreliosis. *The Lancet*, 379(9814):461–473, 2012.

[79] Vanessa V. Angelova Steven M. Singer#, Marc Y. Fink. HHS Public Access. *Physiology & behavior*, 176(3):139–148, 2019.

[80] Kelly R. Stevens and Charles E. Murry. Human Pluripotent Stem Cell-Derived Engineered Tissues: Clinical Considerations. *Cell Stem Cell*, 22(3):294–297, 2018.

[81] Brandee L. Stone, Yvonne Tourand, and Catherine A. Brissette. Brave New Worlds: The Expanding Universe of Lyme Disease. *Vector-Borne and Zoonotic Diseases*, 17(9):619–629, 2017.

[82] Abraham D Stroock, Stephan K W Dertinger, Armand Ajdari, Igor Mezić, A Howard, George M Whitesides, Armand Ajdari, Igor Mezic, and Howard A Stone. Chaotic Mixer for Microchannels Published by

: American Association for the Advancement of Science Stable URL : http://www.jstor.org/stable/3075690 REFERENCES Linked references are available on JSTOR for this article : You may need to log in to JSTOR to a. 295(5555):647–651, 2016.

[83] D. James Surmeier, José A. Obeso, and Glenda M. Halliday. Selective neuronal vulnerability in Parkinson disease. *Nature Reviews Neuroscience*, 18(2):101–113, 2017.

[84] Kazutoshi Takahashi, Koji Tanabe, Mari Ohnuki, Megumi Narita, Tomoko Ichisaka, Kiichiro Tomoda, and Shinya Yamanaka. Induction of Pluripotent Stem Cells from Adult Human Fibroblasts by Defined Factors. *Cell*, 131(5):861–872, 2007.

[85] Kazutoshi Takahashi and Shinya Yamanaka. Induction of Pluripotent Stem Cells from Mouse Embryonic and Adult Fibroblast Cultures by Defined Factors. *Cell*, 126(4):663–676, 2006.

[86] Chad Tang, Andrew S Lee, Jens-Peter Volkmer, Debashis Sahoo, Divya Nag, Adriane R Mosley, Matthew A Inlay, Reza Ardehali, Shawn L Chavez, Renee Reijo Pera, Barry Behr, Joseph C Wu, Irving L Weissman, and Micha Drukker. An antibody against SSEA-5 glycan on human pluripotent stem cells enables removal of teratoma-forming cells. *Nature biotechnology*, 29(9):829–34, 2011.

[87] Mark H. Tuszynski, Leon Thal, Mary Pay, David P. Salmon, Hoi Sang U, Roy Bakay, Piyush Patel, Armin Blesch, H. Lee Vahlsing, Gilbert Ho, Gang Tong, Steven G. Potkin, James Fallon, Lawrence Hansen, Elliott J. Mufson, Jeffrey H. Kordower, Christine Gall, and James Conner. A phase 1 clinical trial of nerve growth factor gene therapy for Alzheimer disease. *Nature Medicine*, 11(5):551–555, 2005.

[88] Bettina Wagner, Heather Freer, Alicia Rollins, David Garcia-Tapia, Hollis N. Erb, Christopher Earnhart, Richard Marconi, and Patrick Meeus. Antibodies to Borrelia burgdorferi OspA, OspC, OspF, and C6 antigens as markers for early and late infection in dogs. *Clinical and Vaccine Immunology*, 19(4):527–535, 2012.

[89] Kyle Wellmerling, Christian Lehmann, Ankur Singh, and Brian J. Kirby. Microfluidic chip for label-free removal of teratoma-forming cells from therapeutic human stem cells. *Journal of Immunology and Regenerative Medicine*, 10(December 2019):100030, 2020.

[90] Gary P. Wormser. Hematogenous dissemination in early Lyme disease. *Wiener Klinische Wochenschrift*, 118(21-22):634–637, 2006.

[91] Xiaofeng Yang, Martin S. Goldberg, Taissia G. Popova, George B. Schoeler, Stephen K. Wikel, Kayla E. Hagman, and Michael V. Norgard. Interdependence of environmental factors influencing reciprocal patterns of gene expression in virulent Borrelia burgdorferi. *Molecular Microbiology*, 37(6):1470–1479, 2000.